Finite Element Modelling of the Time-dependent Potash Mining Process

by

Nana Mulyana

A thesis
Submitted to the Faculty of Graduate Studies
in Partial Fulfillment of the Requirements
for the Degree of

MASTER OF SCIENCE

Department of Civil Engineering
University of Manitoba
Winnipeg, Manitoba

ISBN 0-315-78004-5

FINITE ELEMENT MODELLING OF THE TIME-DEPENDENT POTASH MINING PROCESS DEVELOPMENT

BY

NANA MULYANA

A Thesis submitted to the Faculty of Graduate Studies of the University of Manitoba in partial fulfillment of the requirements for the degree of

MASTER OF SCIENCE

Abstract

For centuries man has been created openings deep down below the ground surface to exploit potash as a commodity. Most often underground openings are located based on human instinct and experience. This can frequently lead to error, and a reliable rational, numerical method for locating these openings is required. Since two of the major problems in potash mining are time-dependent room closure and pillar yielding, this thesis investigates the applicability of elasto-viscoplasticity in modelling the material and predicting its behaviour.

After reviewing existing literature, a robust computational scheme for analyzing time-dependent problem in potash has been developed. The program is designed to include four widely used yield criteria, an implicit time integration scheme, and an overlay system.

Finally, two case studies are undertaken. The first case study is a simulation of uniaxial creep strain of Patience Lake (Lanigan) potash under various levels of applied stress. The second case study is a simulation of time-dependent room closure and pillar yielding of five underground potash caverns in Saskatchewan.

Displacement and stress results of the theoretical analysis are compared with field readings, the numerical model showing promise as a predictor of behaviour of potash under mining excavation.

Acknowledgement

I would like to thank my advisor, Professor John I. Glanville for his guidance during all my years as a graduate student at The University of Manitoba, and for his participation in this study. I would also like to thank Dr. M. L. Ayari for his great guidance, advice, encouragement, patience, and for introducing me to the world of non-linearity, time-dependency, interactive programming, and LaTeXwhich proved to be essential to the successful completion of this engineering study. This research would not be carried out without the experimental evidences, generously provided by Dr. Emery Lajtai and his graduate students. The efforts of Mr. Victor Ong of the Potash Corporation of Saskatchewan in providing the field data are also very appreciated.

I would also like to thank the Board of Directors of the State Electricity Corporation (PLN) of the Republic of Indonesia and Canadian International Development Agency (CIDA) who gave me the opportunity of taking this degree.

I must thank my parents, my dearest wife and my children Prita and Dhany for their infinite love and patience during my study in Canada.

Finally, I would like to thank all my friends for their valued and continuous friendship.

Contents

List of Figures

Chapter 1

Introduction

1.1 Background of Study

For centuries, a great number of underground openings have been made to exploit salt rock as a raw material. Potash is a family of salt rock with high KCl content which makes it a valuable commodity as fertilizer. More recently, because of its low permeability salt rock has been used as a place to store hazardous wastes such as nuclear wastes.

Potash is found abundantly in Saskatchewan at a depth around one km below the ground surface. Although it has been extracted since 1958, little is known of its mechanical response to stress, mining, and time. This research is part of an important academic effort led by Lajtai [18],[19] to understand the mechanical behaviour of potash rock. While this thesis is targeting the time-dependent modeling and the mining sequence, other investigations include fracture characterization[21] [22], constitutive behaviour, and experimental creep testing[20]. The summary of the above research program is presented in reference [24].

1.2 Scope of Study

In general, the behaviour of engineering materials is very complicated. The solution of a practical problem can only be reached through idealization and simplification of the mathematical model representing the true material behaviour. In solid and

structural mechanics, plasticity, which can be considered as a generalization of the theory of elasticity, is still the most sophisticated theory in approaching the behaviour of most common engineering materials.

Many computer programs related to plasticity have been developed with various range of applications. There is no single program existing that can handle the wide range of engineering problems that require resolution. A finite element program based on elasto-viscoplasticity incorporating various failure criteria and various time integration schemes shows promise as a very useful tool for approaching time dependent behaviour. This study utilizes elasto-viscoplasticity to investigate the time-dependent behaviour in potash with multiple underground caverns.

Throughout this study small displacements and strains, linear strain hardening, constant temperature as well as isotropic material properties are adopted. Although three dimensional formulation is used as far as possible, only two dimensional analysis is incorporated into the finite element program.

1.3 Objective of Study

This engineering study is conducted in order to reach the following goals:

- To develop several options to the computer code based on elasto-viscoplasticity which is taken from reference [1], namely:

    1. Several failure criteria that are widely accepted or used, i.e., Tresca, Mohr-Coulomb, Drucker-Prager are embeded and the code is designed such that any failure criteria can be added without undue difficulty.

    2. The implicit time integration scheme for the above criteria is adopted so that larger time steps can be applied without violating the stability requirements.

    3. An overlay model is added to give more flexibility in modelling the complex behaviour of a material.

- To apply the program in the simulation of the following problems:

    1. Simulation of a uniaxial creep test of a Lanigan potash rock.
    2. Simulation of a field test of a mining excavation consisting of five openings, with a particular concern on time-dependent displacement and stress around the openings.

1.4 Thesis Outline

This thesis is organized as follows:

1. The first chapter describes an overview of the scope, goals, and outline of the engineering study.
2. The second chapter is a literature survey which provides an overview of the theories related to this engineering study. Three major topics are covered briefly:
    - linear elasticity
    - plasticity including time-dependent effects
    - time integration schemes of the finite element semi-discrete governing equations.
3. The third chapter presents:
    - finite element formulation of elasto-viscoplasticity for implicit time integration scheme. This implicit scheme is applied with von Mises, Tresca, Mohr-Coulomb, and Drucker-Prager yield criteria
    - development of an interactive numerical process to model mining excavation
    - program organization

4. The fourth chapter contains application of the program to two cases related to time-dependent behaviour in potash mining.

5. The last chapter outlines the conclusion from this research and recommends future work that should be undertaken to improve the numerical model.

Chapter 2

Basic Concepts and Literature Survey

2.1 Introduction

This chapter reviews several basic concepts related to this study and serves as a theoretical background. The theory of plasticity involves the relationship of stress and strain in a deformed body after a part or the entire body has yielded. The plastic behaviour is characterized by an *irreversible straining* or *inelastic deformation* which can be time independent *elasto-plastic behaviour* or time dependent *viscoplastic behaviour*. Obviously, the basic concept of the yielding criteria should be addressed. However, since most engineering materials indicate linearly elastic behaviour before yielding, the basic concept of linear elasticity is also considered.

The composite model so-called overlay system is introduced in order to obtain a better approximation to the complex behaviour of materials, and numerical stability and accuracy are essential to efficient program development.

Thus, this chapter particulary reviews basic concepts of the following topics:

1. Linear elasticity
2. Plasticity
    - Yield criteria
    - Work or strain hardening

- Elasto-plastic stress/strain relationship
- Elasto-viscoplasticity

3. Explicit versus Implicit schemes
4. Overlay Models

2.2 Basic Concept of Linear Elasticity

The material in a body is defined as being *elastic* if upon the release of the applied forces the body recovers its original shape and size. For such materials, the current state of stress depends only on the current state of deformation; that is, the stress is a function of strain and it is called a *Cauchy elastic material* [2]. The constitutive equations are given by

$$\sigma_{ij} = \mathcal{F}_{ij}(\epsilon_{kl}) \tag{2.1}$$

where the $\mathcal{F}_{ij}$ is the *elastic response function.* According to this equation the *elastic* behaviour is *reversible* as well as *path independent.* The behaviour is independent of stress or strain histories.

To ensure that no energy can be generated through load cycles and thermodynamic laws are always satisfied, the above equation is restricted such that

$$\sigma_{ij} = \frac{\partial W}{\partial \epsilon_{ij}} \tag{2.2}$$

where W is the *elastic strain energy* and it generally is a function of ϵ_{ij}.

The material that satisfies both of the above equations is the so-called *hyperelastic* or *Green elastic* material [3].

The simplest and general form for the *linear* constitutive relation of a *Cauchy elastic* material which is also known as the *generalized Hooke's law* is given by

$$\sigma_{ij} = C_{ijkl}\epsilon_{kl} \tag{2.3}$$

where

C_{ijkl} = tensor of material elastic constants

For *isotropic linear hyperelastic* materials, the number of independent constants of an elastic tensor is reduced from 81 to 2 (*Lame's constants*) and the constitutive equation is given by

$$\sigma_{ij} = \lambda \epsilon_{kk} \delta_{ij} + 2\mu \epsilon_{ij} \tag{2.4}$$

where

λ and μ are *Lame's constants*
δ_{ij} is the *Kronecker delta*

The constants λ and μ are usually expressed in other forms of elastic constants which are determined from *experimental tests* of some simple states of stress and strain, such as, hydrostatic compression test, simple tension test, simple shear test, and uniaxial strain test. The relations among the elastic constants can be found in many references.

The following forms of *isotropic linear elastic* constitutive equation are used frequently in practice [2];

$$\sigma_{ij} = \frac{E}{(1+\nu)} \epsilon_{ij} + \frac{\nu E}{(1+\nu)(1-2\nu)} \epsilon_{kk} \delta_{ij} \tag{2.5}$$

$$\sigma_{ij} = 2G\epsilon_{ij} + \frac{3\nu K}{(1+\nu)} \epsilon_{kk} \delta_{ij} \tag{2.6}$$

$$\epsilon_{ij} = \frac{1}{2G} \sigma_{ij} - \frac{\nu}{3K(1-2\nu)} \delta_{ij} \sigma_{kk} \tag{2.7}$$

where;

E = Young's modulus
K = Bulk modulus
G = Shear modulus
ν = Poisson's ratio

2.3 Basic Concept of Plasticity

2.3.1 The Yield Criteria

Plasticity theory requires a hypothesis which indicates the beginning of the onset of plastic flow. In the case of uniaxial loading, the hypothesis is simply the yield stress of the corresponding material. However, for multiaxial loading, the hypothesis should include the effect of all stress components. The critical combination of those stress components at a point of a body which indicates the commencement of plastic flow is defined as *yield criterion or yield condition* [2], [4].

In general, the yield criterion can be expressed as [2], [3], [4], [5], [6];

$$f(\sigma_{ij}) = k(\kappa) \tag{2.8}$$

where f is some function and k is a material parameter to be determined experimentally. The term k may be a function of a hardening parameter κ or a constant. The above equation states that if f is less than the value of the right hand side, elastic behaviour is implied. For *isotropic* materials, equation 2.8 can be expressed either in the form of principal stresses or in the form of stress invariants, since the yield criterion is independent of coordinate axes. Furthermore, experimental evidence [6] indicates that the effect of moderate hydrostatic stress on plastic deformation is negligible and, therefore, the yield criteria can be also expressed in term of invariants of deviatoric stresses.

A yield surface is a geometrical representation of a yield criterion in the principal stress space. This surface is developed by considering all stress combinations which can cause yielding. The shape of this surface depends on the particular yield criteria under consideration. Points within this surface are considered to be elastic, while points on this surface correspond to perfectly plastic behaviour, and points outside the surface correspond to strain hardening. Since the stress vector at a point can be decomposed into hydrostatic and deviatoric stress components, the deviatoric stresses will lie on the octahedral plane, the so called π plane, and the hydrostatic

stresses will be prependicular to this plane and do not affect the yield criterion.

2.3.1.1 Tresca Yield Criterion

In 1864, Tresca [5] proposed that yielding begins when the maximum shear stress reaches a certain value. If the principle stresses are σ_1, σ_2, σ_3 and assuming $\sigma_1 \geq \sigma_2 \geq \sigma_3$ then yielding begins when

$$\sigma_1 - \sigma_3 = k(\kappa) \tag{2.9}$$

By considering all possible maximum shear stress values, the Tresca yield criterion is representated either by the surface of an infinitely long *hexagonal cylinder* in the principal stress space or by a *hexagonal plane* on the π plane.

The Tresca yield criterion is applicable for metal since it does not depend on the hydrostatic stress.

2.3.1.2 von Mises Yield Criterion

In 1913, Von Mises [5] suggested that yielding occurs when the second invariant of deviatoric stress reaches a critical value, or

$$\sqrt{J_2} = k(\kappa) \tag{2.10}$$

where J_2 is the second deviatoric stress invariant which can be written as

$$\begin{aligned} J_2 &= \tfrac{1}{2}\sigma'_{ij}\sigma'_{ij} \\ &= \tfrac{1}{6}[(\sigma_1 - \sigma_2)^2 + (\sigma_2 - \sigma_3)^2 + (\sigma_3 - \sigma_1)^2] \end{aligned}$$

This yield criterion is representated by an infinitely long *circular cylinder* in the principal stress space or by a *circle* with a radius of $\sqrt{2}\ k$ on π plane.

There are two physical interpretations of the von Mises yield criterion. In 1924, Hencky [6] mentioned that yielding begins when the elastic energy of distortion reaches a critical value. On the otherhand, Nadai (1937) [6] interpreted that yielding begins when the *octahedral shear stress* τ_{oct} reaches a critical value.

The von Mises yield criterion is the most widely used for metals since this law fits the experimental data more closely than Tresca's.

2.3.1.3 Mohr-Coulomb Yield Criterion

This criterion was originally proposed for soils by Coulomb in 1773 [5] and has the form of

$$\tau = c - \sigma_n \tan\phi \tag{2.11}$$

where

c =cohesion
ϕ =angle of internal friction
τ =shearing stress
σ_n =normal stress

According to Mohr (1882) [5], equation 2.11 can be written in the form

$$(\sigma_1 - \sigma_3) = 2c\cos\phi - (\sigma_1 + \sigma_3)\sin\phi \tag{2.12}$$

In the principal stress space, this yield criterion gives a *conical* yield surface which normal section at any point is an *irregular hexagon.* The conical shape of the yield surface means that a hydrostatic stress does influence yielding, which is also evident from the last term of equation 2.11.

The Mohr-Coulomb yield criterion is applicable to concrete, rock and soil problems; however, the predicted tensile strength is overestimated especially when it is applied to concrete [2].

2.3.1.4 Drucker-Prager Yield Criterion

In 1952, Prager [5] presented a modified von Mises yield criterion based on the Mohr-Coulomb approximation. This criterion can be stated as

$$\alpha J_1 + \sqrt{J_2} = k' \tag{2.13}$$

The shape of this yield surface in principal stress space is a *circular cone.* The circle will coincide with the outer apices of the Mohr-Coulomb hexagon when the values of α and k' are

$$\alpha = \frac{2\sin\phi}{\sqrt{(3)}(3 - \sin\phi)} \tag{2.14}$$

$$k' = \frac{6c\cos\phi}{\sqrt{(3)}(3-\sin\phi} \tag{2.15}$$

Coincidence with the inner apices is provided by

$$\alpha = \frac{2\sin\phi}{\sqrt{(3)}(3+\sin\phi)} \tag{2.16}$$

$$k' = \frac{6c\cos\phi}{\sqrt{(3)}(3+\sin\phi} \tag{2.17}$$

Again, this yield criterion is applicable to concrete, rock, and soil.

2.3.2 Work or strain hardening

Formulating physical relations which describe the actual behaviour of a material during plastic flow is a very complex problem. This is due to nonlinearity, irreversibility of deformation processes and to a number of phenomena which occur after the material has become plastic, such as time dependency. Since it was mentioned by Olzak et. al [7], it still holds true that the theory of plasticity is developed from hypotheses and assumptions of a phenomenological character based on certain observations and experimental investigations.

Several models had been developed based on the dependency of stress levels at which further plastic deformation occurs to the current degree of plastification or plastic straining. Figure 2.1 shows that the yield stress level of a *perfectly plastic* material does not depend on the degree of plastification. An *isotropic strain hardening* material is defined when the subsequent yield surfaces are a uniform expansion of the original yield surface without translation, as shown in Figure 2.2. For a *kinematic hardening* material, the subsequent yield surfaces preserve their shape and orientation but translate as a rigid body as shown in Figure 2.3. The kinematic hardening model is raised from the experimentally observed *Bauschinger effect* on cyclic loading. If the subsequent yield surfaces contract uniformly as shown in Figure 2.4 then the material is said to be *isotropically strain soften.*

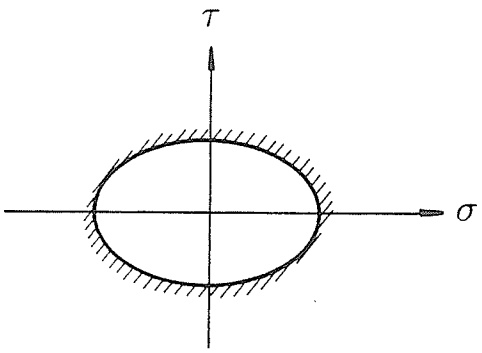

Figure 2.1: Perfectly plastic

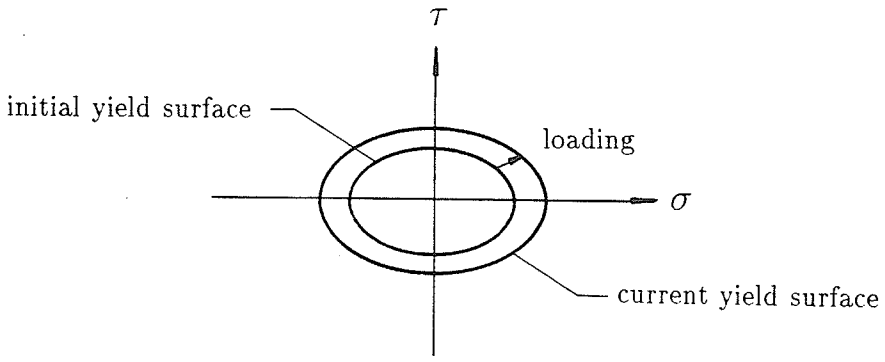

Figure 2.2: Isotropic strain hardening

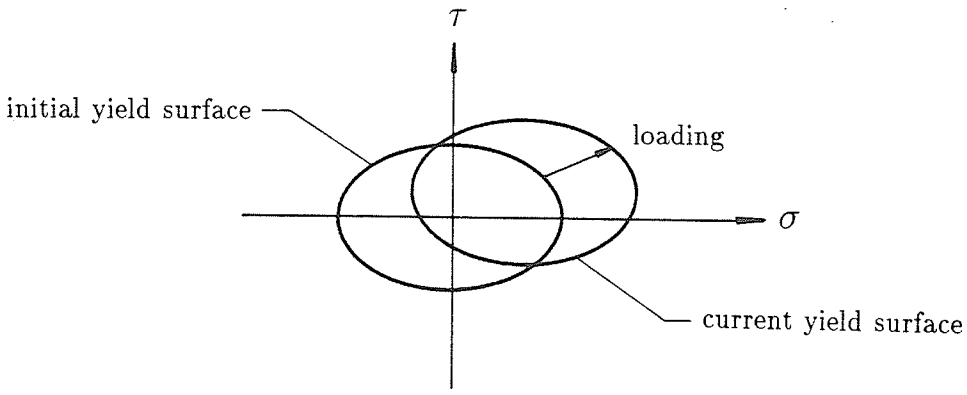

Figure 2.3: Kinematic strain hardening

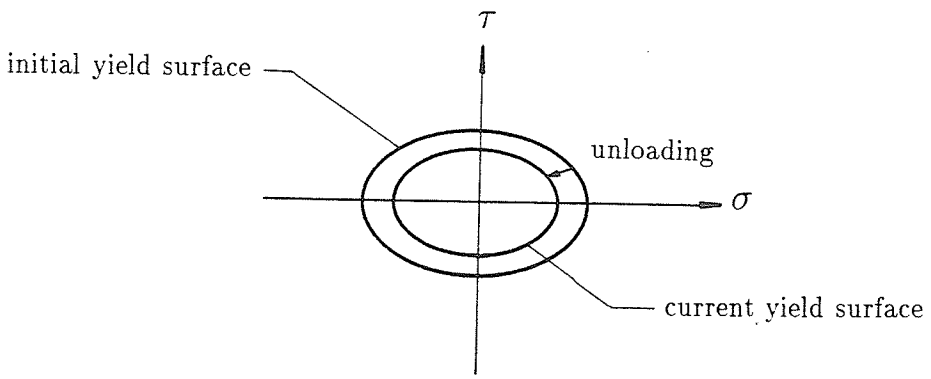

Figure 2.4: Isotropic strain softening

In this study only the *isotropic linear strain hardening* will be applied. The strain hardening can be defined by relating the yield stress k to the plastic deformation by means of the hardening parameter κ of equation 2.8 in two ways [7], [6], [8]. The first hypothesis states that the degree of work hardening can be postulated to be a function of the *total plastic work* W_p, as given by [6],

$$\kappa = W_p \tag{2.18}$$

where

$$W_p = \int \sigma_{ij}(d\epsilon_{ij})_p$$

and $(d\epsilon_{ij})_p$ are the increments of plastic strain. Another hypothesis states that κ can be related to the *total plastic deformation* in terms of *effective plastic strain* $\bar{\epsilon}_p$ [6] as

$$\kappa = \bar{\epsilon}_p \tag{2.19}$$

where

$$\bar{\epsilon}_p = \int \sqrt{[\tfrac{2}{3}(d\epsilon'_{ij})_p(d\epsilon'_{ij})_p]}$$

The hypotheses of equation 2.18 and equation 2.19 for the flow theory have been proved by Hill to be equivalent [8].

2.3.3 Elasto-plastic stress/strain relation

After the work hardening law has been set, a relation between the plastic deformation and the stress history has to be established. Essentially, there are two different

types of those relations. The first relation is the basis of the *deformation theory* and the second gave rise to the popular *flow theory* of plasticity.

2.3.3.1 Deformation Theory

The total strain is composed of elastic and plastic parts; that is, $\epsilon_{ij} = (\epsilon_{ij})_e + (\epsilon_{ij})_p$. The elastic strain is expressed as in equation 2.3. In 1924 Hencky extended the total strain theory of elasticity to plasticity as given by [4], [7], [8]

$$(\epsilon_{ij})_p = F(J_2)\sigma'_{ij} \quad (dJ_2 >< 0) \tag{2.20}$$

where $F(J_2)$ is a tensor operator made out of scalar quantities. The positive and negative inequalities indicate loading and unloading respectively. The above equation means that *total* plastic strains are propotional to the deviatoric stress components. For a neutral stress variation $dJ_2 = 0$, that is perfectly plastic condition, equation 2.3 and equation 2.20 can be written in incremental form [7] as

$$d(\epsilon_{ij})_e = \mathcal{F}_{ijkl} d\sigma_{kl} \tag{2.21}$$

$$d(\epsilon_{ij})_p = F(J_2) d\sigma'_{ij} \tag{2.22}$$

Equation 2.21 and equation 2.22 give two different values of strain increment for a neutral stress variation.

Thus, the deformation theory is considered unsuitable to describe the complete plastic behaviour for the following reasons [7], [4], [8]:

- The relation of strain to stress is *unique* since the final state of strain is determined by the final state of stress, which is not true for plastic behaviour [4], [8].
- *A priori* assumptions to loading and unloading have to be laid in order to get the solution [7].
- No continuity between elastic and plastic region is found for neutral change of stress [7], [8].

2.3.3.2 Flow Theory

Considering the plastic state, $f = k$, for the incremental change of stress $d\sigma_{ij}$, the increment of the yield surface is [6], [8]

$$df = \frac{\partial f}{\partial \sigma_{ij}} d\sigma_{ij} \quad = \frac{\partial f}{\partial J_2} dJ_2, \tag{2.23}$$

where f is the yield criterion in the form of a function of the second invariant of deviatoric stress.

Then if;

$df = 0$, neutral loading (perfectly plastic behaviour) and the stress point remains on the yield surface.
$df > 0$, plastic loading (isotropic strain hardening).
$df < 0$, elastic unloading (linear elastic behaviour).

In order to remove the discontinuity between loading and unloading regions then the $d(\sigma_{ij})_p$ should be zero, or one may write [8]

$$d(\sigma_{ij})_p = G_{ij} df \tag{2.24}$$

where G_{ij} is a symmetric tensor which is generally a function of the stress components and previous strain history and should satisfy two conditions [8];

- G_{ii} should be equal to zero since hydrostatic stresses have no significant effect on plastic volume change (incompressibility).
- Since the material is isotropic, the principal axes of the plastic strain increment should coincide with the principal stress axes.

It was Melan in 1938 who first used the G_{ij} which can satisfy the above condition, in the form of [8]

$$d(\epsilon_{ij})_p = h \frac{\partial Q}{\partial \sigma_{ij}} df \tag{2.25}$$

where Q and h are scalar function of the deviatoric stress invariants.

Furthermore, by the assumption that *the plastic strain increment is proportional to the stress gradient of the plastic potential* Q, equation 2.25 can be written as [6]

$$d(\epsilon_{ij})_p = d\lambda \frac{\partial Q}{\partial \sigma_{ij}} \tag{2.26}$$

where $d\lambda$ is a proportionality constant called the *plastic multiplier*. Equation 2.26 is known as the *flow rule*.

Since both f and Q are functions of the deviatoric invariants, then the case of $Q = f$ is considered to be valid. This assumption is called the *associated* theory of plasticity and equation 2.26 becomes

$$d(\epsilon_{ij})_p = d\lambda \frac{\partial f}{\partial \sigma_{ij}} \tag{2.27}$$

The term $\frac{\partial f}{\partial \sigma_{ij}}$ is a vector directed normal to the yield surface and it is called the *normality condition*. If $f = J_2'$, equation 2.27 is known as the *Prandtl-Reuss* equation of the form [6]

$$d(\epsilon_{ij})_p = d\lambda \sigma_{ij}' \tag{2.28}$$

The complete incremental relationship between stress and strain for elasto-plastic is given as [6]

$$d\epsilon_{ij} = \frac{\sigma' ij}{2G} + \frac{(1-2\nu)}{E}\delta_{ij}\sigma_{kk} + d\lambda \frac{\partial f}{\partial \sigma_{ij}} \tag{2.29}$$

2.3.4 Elasto-viscoplasticity

Generally, time dependence of inelastic deformation is always present to some degree. Elasto-viscoplasticity allows the modelling of time rate effects in the plastic deformation process as well as in the elastic deformation process. The latter phenomenon is so-called creep, which is nothing but redistribution of stress and/or strains with time under elastic material response. These two phenomena cannot be

distinguished by experimentation and their separation is largely intended for analytical convenience only. As it will be shown in the next chapter, elasto-viscoplasticity can models both effects and elasto-plasticity as well [6], [12].

2.3.4.1 One dimension rheological model

The concept of elasto-viscoplasity is best introduced by a one-dimensional rheological model, as illustrated in Figure 2.5. The model consists of a linear spring, a dashpot, and a friction slider component. The total strain of the model can be divided into *elastic* and *viscoplastic* components as

$$\epsilon = \epsilon_e + \epsilon_{vp} \tag{2.30}$$

The total stress σ is equal to the stress in the spring σ_e and it is equal to the sum of stresses in the dashpot and in the slider as

$$\sigma = \sigma_e = \sigma_d + \sigma_p = E\epsilon_e \tag{2.31}$$

where E is elastic modulus of the spring.

The friction slider only becomes active if its stress component σ_p is equal to or larger than some limiting stress value Y. The limiting value Y is nothing but the stress level of which the onset of viscoplasticity begins. This Y can also have the strain-hardening characteristics of the material and is given as

$$Y = \sigma_y + H'\epsilon_{vp} \tag{2.32}$$

where σ_y is *uniaxial yield stress*, H' is the slope of the *strain hardening* portion of the stress-strain curve without the elastic strain component. Thus, the stress in the friction slider is

$\sigma_p = \sigma$ if $\sigma_p < Y$
$\sigma_p = Y$ if $\sigma_p \geq Y$

The stress in the dashpot depends on the viscoplastic strain rate which is expessed as

$$\sigma_d = \mu \frac{d\epsilon_{vp}}{dt} \tag{2.33}$$

where μ is the *viscosity coefficient.*

The stress-strain relationship for the elastic condition is found by using equation 2.30 and equation 2.31 with $\epsilon_{vp} = 0$ and $\sigma_d = 0$ which leads to:

$$\sigma = E\epsilon \tag{2.34}$$

After the onset of the viscoplastic strain, the stress-strain relationship can be found by using equation 2.30 through equation 2.33, which leads to a first order ordinary differential equation of the form

$$\dot{\epsilon} = \frac{\dot{\sigma}}{E} + \gamma[\sigma - (\sigma_y + H'\epsilon_{vp})] \tag{2.35}$$

where γ is defined as the *fluidity parameter* and it is equal to $\frac{1}{\mu}$. Comparing with equation 2.30, equation 2.35 can be written

$$\dot{\epsilon} = \dot{\epsilon_e} + \dot{\epsilon_{vp}} \tag{2.36}$$

where,

$$\dot{\epsilon_e} = \frac{\dot{\sigma}}{E} \tag{2.37}$$

$$\dot{\epsilon_{vp}} = \gamma[\sigma - (\sigma_y + H'\epsilon_{vp})] \tag{2.38}$$

Equation 2.38 defines the viscoplastic strain rate in terms of the excess of stress from the steady state yield value.

The closed form solution of equation 2.35 for a constant applied stress $\sigma = \sigma_a$ is found to be:

for non zero H'

$$\epsilon = \frac{\sigma_a}{E} + \frac{(\sigma_a - \sigma_y)}{H'}[1 - e^{-H'\gamma t}] \tag{2.39}$$

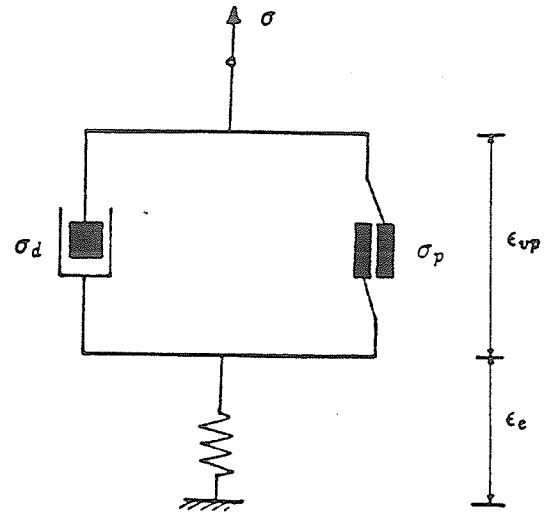

Figure 2.5: One dimensional elasto-viscoplastic rheological model

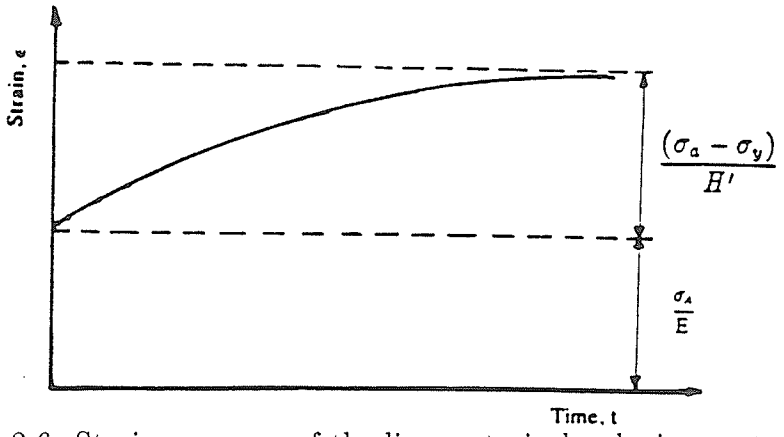

Figure 2.6: Strain response of the linear strain hardening material

for zero H'

$$\epsilon = \frac{\sigma_a}{E} + (\sigma_a - \sigma_y)\dot{\gamma t} \tag{2.40}$$

Graphical representation of the above solutions are shown in Figure 2.6 and Figure 2.7.

2.3.4.2 Multiaxial elasto-viscoplasticity

As in the one dimensional analysis, total strain rate can be composed into the sum of elastic strain rate and viscoplastic strain rate, as given in equation 2.36, except that it is written in vector form, which is indicated by a bold character. The stress

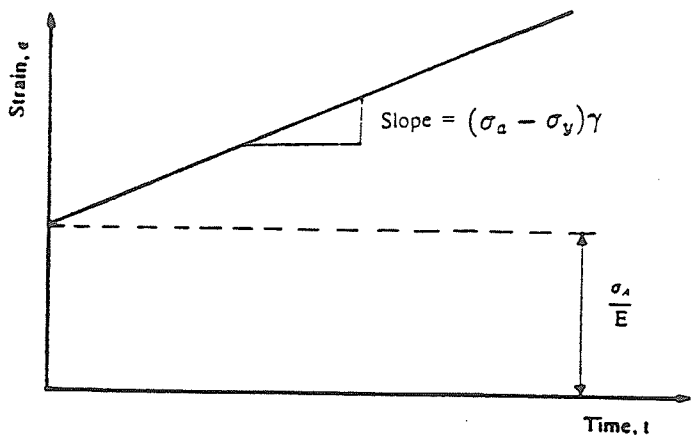

Figure 2.7: Strain response for the perfectly plastic material

rate can be calculated using

$$\dot{\sigma} = \mathbf{D}\dot{\epsilon}_e \tag{2.41}$$

where $\mathbf{D}$ is the elasticity matrix.

The onset of viscoplasticity is assumed to be a scalar yield condition of the form

$$F(\sigma, \epsilon_{vp}) - F_o = 0 \tag{2.42}$$

where $F(\sigma, \epsilon_{vp})$ is a scalar function obtained from one of the equations in section 2.3.5 which indicates the level of stress due to the applied forces. F_o is the uniaxial yield stress which indicates the beginning of the viscoplastic behaviour and its value is determined experimentally. The viscoplastic flow occurs when the values of $F > F_o$ only.

The viscoplastic strain rate cannot be defined as in the one dimensional cases since the stress and strain are the vectorial forms. Therefore the specific formulation defining the viscoplastic strain rate has to be chosen. One of the viscoplastic strain rate formulations that has wide applicability is the one which has been proposed by Perzyna [9] as

$$\dot{\epsilon}_{vp} = \gamma < \Phi(F) > \frac{\partial Q}{\partial \sigma} \tag{2.43}$$

where

Q = plastic potential

γ = fluidity parameter
$< \Phi(F) >=$ a positive monotonic increasing function
$\Phi(F) > 0$ if $F > 0$
$\Phi(F) = 0$ if $F \leq 0$

For the associated plasticity, Q can be assumed to be equal to F and equation 2.43 can be written as

$$\dot{\epsilon}_{vp} = \gamma < \Phi(F) > \frac{\partial F}{\partial \boldsymbol{\sigma}} = \gamma < \Phi(F) > \mathbf{a} \tag{2.44}$$

where $\mathbf{a}$ is termed *flow vector* and its direction is normal to the yield surface. Many forms of the Φ function have been proposed, some of the most common version being

$$\Phi(F) = \left(\frac{F - F_o}{F_o}\right)^i \tag{2.45}$$

$$\Phi(F) = e^{j(\frac{F-F_o}{F_o})} - 1 \tag{2.46}$$

$$\Phi(F) = \left(\frac{F}{F_o}\right)^k \tag{2.47}$$

$$\Phi(F) = (F)^l \tag{2.48}$$

in which i, j, k, and l are arbitrary prescribed constants.

2.3.4.3 Strain increment and time integration schemes

Since viscoplasticity is a transient phenomenon, it is essential to determine the viscoplastic strain increment for every time interval throughout the time of interest. Using the general form of incremental quantities over a time interval $\Delta t_n = t_{n+1} - t_n$, the viscoplastic strain increment can be defined using a finite difference formula of the form [6]

$$\Delta \epsilon_{vp}^n = \Delta t_n[(1 - \Theta)\dot{\epsilon}_{vp}^n + \Theta \dot{\epsilon}_{vp}^{n+1}] \tag{2.49}$$

in which Θ is the implicitness parameter. The value of $\Theta = 0$ expresses the *Euler* or *explicit* time integration scheme where $\Theta = 1$ refers to a *fully implicit* scheme and $\Theta = 0.5$ refers to an *implicit trapezoidal* scheme.

For an explicit time integration scheme the process is found to be stable if the values of Δt_n are less than some critical value. Cormeau [10] developed this *critical time step length* theoretically based on $\Phi(F) = F$ for Tresca, Mises, Mohr-Coulomb, and Drucker-Prager yield criteria.

The implicit time integration schemes yield unconditionally stable solution processes. However, these schemes require the determination of the unknown quantity $\Delta\dot{\epsilon}_{vp}^{n+1}$ beforehand. This quantity can be estimated by using a limited Taylor series expansion and one may write

$$\dot{\epsilon}_{vp}^{n+1} = \dot{\epsilon}_{vp}^{n} + \mathbf{H}^n \Delta\boldsymbol{\sigma}^n \tag{2.50}$$

where,

$$\mathbf{H}^n = (\frac{\partial\dot{\epsilon}_{vp}}{\partial\boldsymbol{\sigma}})^n \tag{2.51}$$

Equation 2.49 is now written as

$$\Delta\epsilon_{vp}^{n} = \dot{\epsilon}_{vp}^{n}\Delta t_n + \mathbf{C}^n \Delta\boldsymbol{\sigma}^n \tag{2.52}$$

where,

$$\mathbf{C}^n = \Theta\Delta t_n \mathbf{H}^n \tag{2.53}$$

2.3.4.4 Stress increments

The $\Delta\boldsymbol{\sigma}$ is the stress change occuring in the time interval (stress increment) and is given as

$$\Delta\boldsymbol{\sigma} = \mathbf{D}\boldsymbol{\epsilon}_e^n = \mathbf{D}(\Delta\boldsymbol{\epsilon}^n - \Delta\boldsymbol{\epsilon}_{vp}^n) \tag{2.54}$$

The total strain increment $\Delta\boldsymbol{\epsilon}^n$ can be expressed in terms of the displacement increment. Therefore, equation 2.54 has the form

$$\Delta\boldsymbol{\sigma}^n = \hat{\mathbf{D}}^n(\mathbf{B}\Delta\mathbf{d}^n - \dot{\boldsymbol{\epsilon}}^n_{vp}\Delta t_n) \tag{2.55}$$

with,

$$\hat{\mathbf{D}}^n = (\mathbf{D}^{-1} + \mathbf{C}^n)^{-1} \tag{2.56}$$

2.3.4.5 Equilibrium equation and displacement increment

The equilibrium of forces at any instant of time, t_n should be satisfied according to the following equation

$$\Psi^n = \int_\Omega \mathbf{B}^T\boldsymbol{\sigma}^n d\Omega + \mathbf{f}^n = 0 \tag{2.57}$$

where $\mathbf{f}^n$ is the consistent load vector due to applied forces. This equilibrium condition should be satisfied also during a time increment according to the incremental form of equation 2.57 as

$$\Delta\Psi^n = \int_\Omega \mathbf{B}^T\Delta\boldsymbol{\sigma}^n d\Omega + \Delta\mathbf{f}^n = 0 \tag{2.58}$$

In order to meet the above condition, the displacement increment during any time interval, Δt_n, should be calculated as

$$\Delta\mathbf{d}^n = [\mathbf{K}^n_T]^{-1}\Delta\mathbf{V}^n \tag{2.59}$$

where $\Delta\mathbf{V}^n$ is called as *incremental pseudo-load* [6] of the form

$$\Delta\mathbf{V}^n = \int_\Omega \mathbf{B}^T\hat{\mathbf{D}}^n\dot{\boldsymbol{\epsilon}}^n_{vp}\Delta t_n d\Omega + \Delta\mathbf{f}^n \tag{2.60}$$

$\mathbf{K}^n_T$ is known as the *tangential stiffness matrix* and it is defined as

$$\mathbf{K}^n_T = \int_\Omega \mathbf{B}^T\hat{\mathbf{D}}^n\mathbf{B}d\Omega \tag{2.61}$$

2.3.4.6 Equilibrium correction

The calculated stress increment in equation 2.55 is based on a linearised form of the incremental equilibrium of equation 2.58. Therefore, the total stress $\boldsymbol{\sigma}^{n+1} = \boldsymbol{\sigma}^n + \Delta\boldsymbol{\sigma}^n$ at the end of a time increment is not exactly correct. Consequently, the equilibrium condition of equation 2.57 which is based on the total stress will not be satisfied. The correction to this equilibrium condition should be applied in order to minimize the error. There are several methods available [11], one of the simplest method being called the *residual force method.* In this method the out-of-balance forces Ψ^{n+1} are calculated using equation 2.57 and this force is then added to the incremental pseudo loads for use in the next time step. Alternatively, an iterative process must be applied to retain the out-of-balance force to within an allowable tolerance.

2.3.4.7 Convergence criteria

The convergence to a steady state condition is determined based on the effective viscoplastic strain which occurs at the end of the time increment. The solution is said to be near a steady state condition if the effective viscoplastic strain ratio at the end of any time to first time step is less or equal to some prescribed value. The ratio is calculated for all Gauss integration points. The above criteria can be written as [6]

$$\frac{\Delta t_{n+1} \sum \bar{\dot{\epsilon}}_{vp}^{n+1}}{\Delta t_1 \sum \bar{\dot{\epsilon}}_{vp}^{1}} 100 \leq T \tag{2.62}$$

in which T is a prescribed tolerance factor and $\bar{\dot{\epsilon}}_{vp}$ is the effective viscoplastic strain rate defined as

$$\bar{\dot{\epsilon}}_{vp} = \sqrt{\frac{2}{3}(\dot{\epsilon}_{ij})_{vp}(\dot{\epsilon}_{ij})_{vp}} \tag{2.63}$$

2.3.4.8 Computational procedures

At the beginning of the process or at time $t = 0$, the static elastic analysis is performed by using the value of $\Delta t_0 = 0$ and the resulting quantities $\mathbf{d}^0$, F^0, $\boldsymbol{\epsilon}^0$, $\boldsymbol{\sigma}^0$, and $\boldsymbol{\epsilon}^0_{vp} = 0$ are known.

The main steps in the solution process of the elasto-viscoplastic model can be summarized as follows

Stage 1.

At an arbitrary time $t = t_n$ the equilibrium condition is reached and $\mathbf{d^n}$, $\boldsymbol{\sigma}^n$, $\boldsymbol{\epsilon}^n$, $\boldsymbol{\epsilon}^n_{vp}$, F^n, and Δt_n are known. These quantities are assembled at the beginning of the time step:

- $\mathbf{H}^n$ as in equation 2.51
- $\hat{\mathbf{D}}^n$ as in equation 2.56
- $\mathbf{K}^n_T$ as in equation 2.61
- $\dot{\boldsymbol{\epsilon}}^n_{vp}$ as in equation 2.44
- $\Delta \mathbf{d}^n$ as in equation 2.59
- $\Delta \boldsymbol{\sigma}^n$ as in equation 2.55

Stage 2.

These quantities are assembled at the end of the time step:

- $\mathbf{d}^{n+1} = \mathbf{d}^n + \Delta \mathbf{d}^n$ or total displacements
- $\boldsymbol{\sigma}^{n+1} = \boldsymbol{\sigma}^n + \Delta \boldsymbol{\sigma}^n$ or total stresses
- $\dot{\boldsymbol{\epsilon}}^{n+1}_{vp}$ as in equation 2.44
- Ψ^{n+1} as in equation 2.57

- $\mathbf{V}^{n+1} = \mathbf{V}^n + \Psi^{n+1}$ or incremental pseudo loads

Stage 3.

Apply the convergence criteria according to equation 2.62. If the criteria are satisfied the analysis is terminated. Otherwise, return to Stage 1.

2.4 Explicit versus Implicit scheme

The visco-plasticity analyses require iterative or time integration algorithms for obtaining the solutions. Many researchers have addressed minimizing the computational cost by maximizing the time step [13]. Cormeau [10] obtained the theoretical upper bounds on the time step for explicit/ Euler -type algorithms. In 1978 Hughes and Taylor [14] developed an unconditionally stable implicit algorithm. Later, in 1984, Marques and Owen [15] developed an implicit-explicit time marching scheme. In order to compare both schemes, consider the numerical properties of equation [13];

$$\frac{dy}{dt} = -\eta y \tag{2.64}$$

The explicit numerical approximation for the above equation may be expressed by

$$y^{n+1} = (1 - \Delta t_n \eta) y^n \tag{2.65}$$

or, by the implicit schemes as

$$y^{n+1} = \frac{y^n}{(1 + \Delta t_n \eta)} \tag{2.66}$$

From equation 2.65 and equation 2.66, it is evident that the implicit time integration scheme is unconditionally stable for any value of Δt_n. However, the lack of accuracy become prominent for large time steps.

In equation 2.65, the explicit scheme is stable for $1/\eta \leq \Delta t_n \leq 2/\eta$.

- As Δt_n approaches $\Delta t_{critical} = 2/\eta$, the solution leads to oscillatory stable convergence.

- As Δt_n approaches $\Delta t_{maximum} = 1/\eta$, the solution leads to non-oscillatory stable convergence.

The $\Delta t_{critical}$ is usually used since the steady-state solution is of prime concern. However, some problems the intermediate solution is as important as the steady-state solution. Thus, the numerical stability and accuracy of the explicit time integration scheme is very sensitive to the choice of Δt_n. Furthermore, smaller time steps lead to higher computer costs.

2.5 Overlay models

The simple rheological elasto-viscoplastic model as described previously often fails in approximating the complex behaviour of materials. In 1974, Owen *et al* [16] proposed *the overlay systems* in elasto-plastic finite element analysis and in 1975 Pande *et al* [17] extended it into elasto-viscoplastic modeling.

The basic concept of overlay systems is that a continuum may consist of several layers called *overlays* which undergo the same deformation. In other words, the overlay system consists of several simple models connected in parallel. In finite element applications, this condition can be representated by assembling several layers with the same shapes, coordinates, and boundary conditions one on top of the others. The thickness and material properties of each layer may be different, resulting in a different stress field in each layer. The total stress field is calculated by the sum of the contribution of each layer according to the layer thickness as

$$\boldsymbol{\sigma} = \sum_{i=1}^{n} \boldsymbol{\sigma}_i t_i \tag{2.67}$$

where n is the total number of overlays and should satisfy;

$$\sum_{i=1}^{n} t_i = 1 \tag{2.68}$$

The equilibrium equation 2.57 which should be satisfied becomes

$$\sum_{i=1}^{n} \int_{\Omega} \mathbf{B}^T \boldsymbol{\sigma}_i^n t_i d\Omega + \mathbf{f}_i^n = \mathbf{0} \tag{2.69}$$

The element stiffness matrix of equation 2.61 become

$$\mathbf{K}_T^n = \sum_{i=1}^{n} \int_{\Omega} \mathbf{B}^T \hat{\mathbf{D}}_i^n \mathbf{B} d\Omega \tag{2.70}$$

The physical interpretation of the overlay model in the two-dimensional situation can best be introduced by composite materials. However, the overlay model is nothing but the weighting parameter for combining the contribution of the individual overlays. Thus this concept can further be adopted into three dimensional situations [6],[16],[17].

The application of an overlay system into finite element analysis makes it more powerful. Standard Maxwell viscoelastic, standard Kelvin viscoelastic, and other complex parallel models can be created by the elasto-viscoplastic model along with the overlay system.

Chapter 3

Topics on Finite Element Modelling of Elasto-viscoplasticity

3.1 Implicit scheme formulation

In order to incorporate the implicit time integration algorithm into the program, its formulation should be derived. Firstly, the evaluation of matrix $\mathbf{H}^n$ of equation 2.44 will be performed in a generalized form. Since it involves the flow vector which depends on the yield criterion being considered, the alternative forms of the yield criteria as a function of stress invariants will also be reviewed. Finally, all the neccessary constants will be listed.

3.1.1 Evaluation of matrix $\mathbf{H}^n$

The implicit time integration scheme requires the evaluation of matrix $\mathbf{H}^n$ as expressed in equation 2.51. $\mathbf{H}^n$ should be determined for any assumed yield criterion. From equation 2.44 and dropping superscript n and symbol $<>$ for simplification, matrix $\mathbf{H}^n$ can be expressed as;

$$\mathbf{H} = \frac{\partial \dot{\epsilon}_{vp}}{\partial \boldsymbol{\sigma}} = \gamma(\Phi \frac{\partial \mathbf{a}^T}{\partial \boldsymbol{\sigma}} + \frac{d\Phi}{dF}\mathbf{a}\mathbf{a}^T) \tag{3.1}$$

Since the term $\frac{d\Phi}{dF}$ is a scalar quantity, therefore, essentially, the evaluation of ma-

trix $\mathbf{H}^n$ needs explicit determination of $\frac{\partial \mathbf{a}^T}{\partial \boldsymbol{\sigma}}$ and $\mathbf{a}\mathbf{a}^T$. Matrix $\mathbf{a}$ is the flow vector according to the yield criterion considered.

The yield criterion can be written in the generalized form

$$F(J_1, J_2'^{1/2}, J_3, \theta) = \sigma_y(k) \tag{3.2}$$

Differentiating F with respect to $\boldsymbol{\sigma}$, we obtain

$$\mathbf{a}^T = \frac{\partial F}{\partial \boldsymbol{\sigma}} = \frac{\partial F}{\partial J_1}\frac{\partial J_1}{\partial \boldsymbol{\sigma}} + \frac{\partial F}{\partial J_2'^{1/2}}\frac{\partial J_2'^{1/2}}{\partial \boldsymbol{\sigma}} + \frac{\partial F}{\partial J_3}\frac{\partial J_3}{\partial \boldsymbol{\sigma}} + \frac{\partial F}{\partial \theta}\frac{\partial \theta}{\partial \boldsymbol{\sigma}} \tag{3.3}$$

where,

$$\boldsymbol{\sigma}^T = \{\sigma_x\ ,\ \sigma_y\ ,\ \sigma_z\ ,\ \tau_{yz}\ ,\ \tau_{zx}\ ,\ \tau_{xy}\} \tag{3.4}$$

and θ is defined as

$$\sin 3\theta = -\frac{4J_3}{r^3} = \frac{-3\sqrt{3}}{2}\frac{J_3}{J_2'^{3/2}}. \tag{3.5}$$

Differentiating equation 3.5

$$\frac{\partial}{\partial \boldsymbol{\sigma}}(\sin 3\theta) = -\frac{3\sqrt{3}}{2}\frac{\partial}{\partial \boldsymbol{\sigma}}\left(\frac{J_3}{J_2'^{3/2}}\right)$$

we obtain

$$\begin{aligned} 3\cos 3\theta\left(\frac{\partial \theta}{\partial \boldsymbol{\sigma}}\right) &= \frac{-3\sqrt{3}}{2J_2'^3}\left[\left(\frac{\partial J_3}{\partial \boldsymbol{\sigma}}\right)J_2'^{-3/2} - J_3\frac{\partial\left(J_2'^{-3/2}\right)}{\partial \boldsymbol{\sigma}}\right] \\ &= \frac{-3\sqrt{3}}{2J_2'^3}\left[\left(\frac{\partial J_3}{\partial \boldsymbol{\sigma}}\right)J_2'^{-3/2} - J_3\frac{\partial\left((J_2'^{1/2})^{-3}\right)}{\partial J_2'^{1/2}}\left(\frac{\partial J_2'^{1/2}}{\partial \boldsymbol{\sigma}}\right)\right] \\ 3\cos 3\theta\left(\frac{\partial \theta}{\partial \boldsymbol{\sigma}}\right) &= \frac{-3\sqrt{3}}{2J_2'^3}\left[\left(\frac{\partial J_3}{\partial \boldsymbol{\sigma}}\right)J_2'^{-3/2} - J_3(-3)(J_2'^{1/2})^{-4}\left(\frac{\partial J_2'^{1/2}}{\partial \boldsymbol{\sigma}}\right)\right] \end{aligned}$$

or

$$\left(\frac{\partial\theta}{\partial\boldsymbol{\sigma}}\right) = \frac{-\sqrt{3}}{2\cos 3\theta}\left(J_2^{'-9/2}\right)\left(\frac{\partial J_3}{\partial\boldsymbol{\sigma}}\right) - \frac{3\sqrt{3}}{2\cos 3\theta}\left(\frac{J_3}{J_2^{'3/2}}\right)\frac{1}{J_2^{'7/2}}\left(\frac{\partial J_2^{'1/2}}{\partial\boldsymbol{\sigma}}\right)$$

By using equation 3.5;

$$\mathbf{b}^T = \left(\frac{\partial\theta}{\partial\boldsymbol{\sigma}}\right) = \frac{-\sqrt{3}}{2\cos 3\theta}\left(J_2^{'-9/2}\right)\left(\frac{\partial J_3}{\partial\boldsymbol{\sigma}}\right) + \left(\frac{\tan 3\theta}{J_2^{'7/2}}\right)\left(\frac{\partial J_2^{'1/2}}{\partial\boldsymbol{\sigma}}\right) \tag{3.6}$$

Equation 3.3 can be written in the alternative form

$$\mathbf{a}^T = \frac{\partial F}{\partial\boldsymbol{\sigma}} = c_1\,\mathbf{a}_1^T + c_2\,\mathbf{a}_2^T + c_3\,\mathbf{a}_3^T \tag{3.7}$$

where,

$$\mathbf{a}_1^T = \frac{\partial J_1}{\partial\boldsymbol{\sigma}} = \{\,1\,,\,1\,,\,1\,,\,0\,,\,0\,,\,0\,\} \tag{3.8}$$

$$\mathbf{a}_2^T = \left(\frac{\partial J_2^{'1/2}}{\partial\boldsymbol{\sigma}}\right) = \frac{1}{2\sqrt{J_2'}}\left\{\,\sigma_x'\,,\,\sigma_y'\,,\,\sigma_z'\,,\,2\tau_{yz}'\,,\,2\tau_{yz}\,,\,2\tau_{xy}\,\right\} \tag{3.9}$$

$$\mathbf{a}_3^T = \left(\frac{\partial J_3}{\partial\boldsymbol{\sigma}}\right) =$$

$$\left\{\left(\sigma_y'\sigma_z' - \tau_{yz}^2 + \frac{J_2'}{3}\right)\,,\,\left(\sigma_x'\sigma_z' - \tau_{xz}^2 + \frac{J_2'}{3}\right)\,,\,\left(\sigma_x'\sigma_y' - \tau_{xy}^2 + \frac{J_2'}{3}\right)\,,\right.$$

$$\left.2\left(\tau_{xz}\,\tau_{xy} - \sigma_x'\tau_{yz}\right)\,,\,2\left(\tau_{xz}\,\tau_{yz} - \sigma_y'\tau_{xz}\right)\,,\,2\left(\tau_{yz}\,\tau_{xz} - \sigma_z'\tau_{xy}\right)\right\} \tag{3.10}$$

and

$$c_1 = \frac{\partial F}{\partial J_1} \tag{3.11}$$

$$c_2 = \frac{\partial F}{\partial J_2^{'1/2}} - \frac{\tan 3\theta}{J_2^{'1/2}}\left(\frac{\partial F}{\partial\theta}\right) \tag{3.12}$$

$$c_3 = \frac{\partial F}{\partial J_3} - \frac{\sqrt{3}}{2\cos 3\theta}\,J_2^{'(-3/2)}\left(\frac{\partial F}{\partial\theta}\right) \tag{3.13}$$

Vector $\mathbf{b}$ can be expressed in terms of $\mathbf{a}_1$ and $\mathbf{a}_2$;

$$\mathbf{b}^T = \frac{-\sqrt{3}}{2\cos 3\theta}\left(J_2^{'-9/2}\right)\mathbf{a}_3^T + \left(\frac{\tan 3\theta}{J_2^{'7/2}}\right)\mathbf{a}_2^T$$

Utilizing equation 3.7, $\frac{\partial \mathbf{a}^T}{\partial \boldsymbol{\sigma}}$ is found to be;

$$\begin{aligned}
\frac{\partial \mathbf{a}^T}{\partial \boldsymbol{\sigma}} &= c_1\frac{\partial \mathbf{a}_1^T}{\partial \boldsymbol{\sigma}} + c_2\frac{\partial \mathbf{a}_2^T}{\partial \boldsymbol{\sigma}} + c_3\frac{\partial \mathbf{a}_3^T}{\partial \boldsymbol{\sigma}} + \mathbf{a}_1^T\frac{\partial c_1}{\partial \boldsymbol{\sigma}} + \mathbf{a}_2^T\frac{\partial c_2}{\partial \boldsymbol{\sigma}} + \mathbf{a}_3^T\frac{\partial c_3}{\partial \boldsymbol{\sigma}} \\
&= c_1\frac{\partial \mathbf{a}_1^T}{\partial \boldsymbol{\sigma}} + c_2\frac{\partial \mathbf{a}_2^T}{\partial \boldsymbol{\sigma}} + c_3\frac{\partial \mathbf{a}_3^T}{\partial \boldsymbol{\sigma}} \\
&\quad + \mathbf{a}_1^T\left[\frac{\partial c_1}{\partial J_1}\frac{\partial J_1}{\partial \boldsymbol{\sigma}} + \frac{\partial c_1}{\partial J_2^{'1/2}}\frac{\partial J_2^{'1/2}}{\partial \boldsymbol{\sigma}} + \frac{\partial c_1}{\partial \theta}\frac{\partial \theta}{\partial \boldsymbol{\sigma}}\right] \\
&\quad + \mathbf{a}_2^T\left[\frac{\partial c_2}{\partial J_1}\frac{\partial J_1}{\partial \boldsymbol{\sigma}} + \frac{\partial c_2}{\partial J_2^{'1/2}}\frac{\partial J_2^{'1/2}}{\partial \boldsymbol{\sigma}} + \frac{\partial c_2}{\partial \theta}\frac{\partial \theta}{\partial \boldsymbol{\sigma}}\right] \\
&\quad + \mathbf{a}_3^T\left[\frac{\partial c_3}{\partial J_1}\frac{\partial J_1}{\partial \boldsymbol{\sigma}} + \frac{\partial c_3}{\partial J_2^{'1/2}}\frac{\partial J_2^{'1/2}}{\partial \boldsymbol{\sigma}} + \frac{\partial c_3}{\partial \theta}\frac{\partial \theta}{\partial \boldsymbol{\sigma}}\right] \\
&= c_1\frac{\partial \mathbf{a}_1^T}{\partial \boldsymbol{\sigma}} + c_2\frac{\partial \mathbf{a}_2^T}{\partial \boldsymbol{\sigma}} + c_3\frac{\partial \mathbf{a}_3^T}{\partial \boldsymbol{\sigma}} \\
&\quad + \sum_{i=1}^{3}\mathbf{a}_i^T\left[\frac{\partial c_i}{\partial J_1}\mathbf{a}_1^T + \frac{\partial c_i}{\partial J_2^{'1/2}}\mathbf{a}_2^T + \frac{\partial c_i}{\partial \theta}\mathbf{b}^T\right] \qquad (3.14)
\end{aligned}$$

It can be seen clearly that $\frac{\partial \mathbf{a}_1^T}{\partial \boldsymbol{\sigma}} = \mathbf{0}$.

Differentiating equation 3.10 we get

$$\frac{\partial \mathbf{a}_2^T}{\partial \boldsymbol{\sigma}} = \frac{1}{2\sqrt{J_2'}}\mathbf{M}_1 - \frac{1}{4J_2^{'3/2}}\mathbf{M}_2 \qquad (3.15)$$

where

$$\mathbf{M}_1 = \begin{bmatrix} \frac{2}{3} & \frac{-1}{3} & \frac{-1}{3} & 0 & 0 & 0 \\ & \frac{2}{3} & \frac{-1}{3} & 0 & 0 & 0 \\ & & \frac{2}{3} & 0 & 0 & 0 \\ & & & 2 & 0 & 0 \\ & \text{symm.} & & & 2 & 0 \\ & & & & & 2 \end{bmatrix}$$

and

$$\mathbf{M}_2 = \begin{bmatrix} \sigma_x'^2 & \sigma_x'\sigma_y' & \sigma_x'\sigma_z' & 2\sigma_x'\tau_{yz} & 2\sigma_x'\tau_{zx} & 2\sigma_x'\tau_{xy} \\ & \sigma_y'^2 & \sigma_y'\sigma_z' & 2\sigma_y'\tau_{yz} & 2\sigma_y'\tau_{zx} & 2\sigma_y'\tau_{xy} \\ & & \sigma_z'^2 & 2\sigma_z'\tau_{yz} & 2\sigma_z'\tau_{zx} & 2\sigma_z'\tau_{xy} \\ & & & 4\tau_{yz}^2 & 4\tau_{yz}\tau_{zx} & 4\tau_{yz}\tau_{xy} \\ & \text{symm.} & & & 4\tau_{zx}^2 & 4\tau_{zx}\tau_{xy} \\ & & & & & 4\tau_{xy}^2 \end{bmatrix}$$

By differentiating equation 3.10, $\frac{\partial \mathbf{a}_3^T}{\partial \boldsymbol{\sigma}}$ is found to be

$$\frac{\partial \mathbf{a}_3^T}{\partial \boldsymbol{\sigma}} = \mathbf{M}_3 =$$

$$\begin{bmatrix} \frac{4}{9}\sigma_x - \frac{2}{9}\sigma_y - \frac{2}{9}\sigma_z & \frac{-2}{9}\sigma_x - \frac{2}{9}\sigma_y + \frac{4}{9}\sigma_z & \frac{-2}{9}\sigma_x + \frac{4}{9}\sigma_y - \frac{2}{9}\sigma_z & \frac{-4}{3}\tau_{yz} & \frac{2}{3}\tau_{xz} & \frac{2}{3}\tau_{xy} \\ & \frac{-2}{9}\sigma_x + \frac{4}{9}\sigma_y - \frac{2}{9}\sigma_z & \frac{4}{9}\sigma_x - \frac{2}{9}\sigma_y - \frac{2}{9}\sigma_z & \frac{2}{3}\tau_{yz} & \frac{-4}{3}\tau_{xz} & \frac{2}{3}\tau_{xy} \\ & & \frac{-2}{9}\sigma_x - \frac{2}{9}\sigma_y + \frac{4}{9}\sigma_z & \frac{2}{3}\tau_{yz} & \frac{2}{3}\tau_{xz} & \frac{4}{3}\tau_{xy} \\ & & & -2\sigma_x' & 2\tau_{xy} & 2\tau_{xz} \\ & \text{symm.} & & & -2\sigma_y' & 2\tau_{yz} \\ & & & & & -2\sigma_z' \end{bmatrix}$$

The term $\mathbf{a}_i\mathbf{a}_j^T$ for $i = 1,3$ and $j = 1,3$ can be expressed as

$$\mathbf{a}_1\mathbf{a}_1^T = \mathbf{M}_4 = \begin{bmatrix} 1 & 1 & 1 & 0 & 0 & 0 \\ 1 & 1 & 1 & 0 & 0 & 0 \\ 1 & 1 & 1 & 0 & 0 & 0 \\ 0 & 0 & 0 & 0 & 0 & 0 \\ 0 & 0 & 0 & 0 & 0 & 0 \\ 0 & 0 & 0 & 0 & 0 & 0 \end{bmatrix}$$

$$\mathbf{a}_2\mathbf{a}_2^T = \frac{1}{4J_2'}\mathbf{M}_2$$

$$\mathbf{a}_3\mathbf{a}_3^T = \mathbf{M}_5 = \begin{bmatrix} A^2 & AB & AC & AD & AE & AF \\ & B^2 & BC & BD & BE & BF \\ & & C^2 & CD & CE & CF \\ & & & D^2 & DE & DF \\ & \text{symm.} & & & E^2 & EF \\ & & & & & F^2 \end{bmatrix}$$

where,

$$A = a_3(1) = \left(\sigma_y'\sigma_z' - \tau_{yz}^2 + \frac{J_2'}{3}\right)$$

$$B = a_3(2) = \left(\sigma_x'\sigma_z' - \tau_{xz}^2 + \frac{J_2'}{3}\right)$$

$$C = a_3(3) = \left(\sigma_x'\sigma_y' - \tau_{xy}^2 + \frac{J_2'}{3}\right)$$

$$D = a_3(4) = 2\left(\tau_{xz}\,\tau_{xy} - \sigma'_x\tau_{yz}\right)$$

$$E = a_3(5) = 2\left(\tau_{xz}\,\tau_{yz} - \sigma'_y\tau_{xz}\right)$$

$$F = a_3(6) = 2\left(\tau_{yz}\,\tau_{xz} - \sigma'_z\tau_{xy}\right)$$

$$\mathbf{a}_2\mathbf{a}_3^T = \frac{1}{2\sqrt{J'_2}}\mathbf{M}_6 = \frac{1}{2\sqrt{J'_2}}\begin{bmatrix} \sigma'_xA & \sigma'_xB & \sigma'_xC & \sigma'_xD & \sigma'_xE & \sigma'_xF \\ \sigma'_yA & \sigma'_yB & \sigma'_yC & \sigma'_yD & \sigma'_yE & \sigma'_yF \\ \sigma'_zA & \sigma'_zB & \sigma'_zC & \sigma'_zD & \sigma'_zE & \sigma'_zF \\ 2\tau_{yz}A & 2\tau_{yz}B & 2\tau_{yz}C & 2\tau_{yz}D & 2\tau_{yz}E & 2\tau_{yz}F \\ 2\tau_{zx}A & 2\tau_{zx}B & 2\tau_{zx}C & 2\tau_{zx}D & 2\tau_{zx}E & 2\tau_{zx}F \\ 2\tau_{xy}A & 2\tau_{xy}B & 2\tau_{xy}C & 2\tau_{xy}D & 2\tau_{xy}E & 2\tau_{xy}F \end{bmatrix}$$

$$\mathbf{a}_1\mathbf{a}_2^T = \frac{1}{2\sqrt{J'_2}}\mathbf{M}_7 = \frac{1}{2\sqrt{J'_2}}\begin{bmatrix} \sigma'_x & \sigma'_y & \sigma'_z & 2\tau_{yz} & 2\tau_{zx} & 2\tau_{xy} \\ \sigma'_x & \sigma'_y & \sigma'_z & 2\tau_{yz} & 2\tau_{zx} & 2\tau_{xy} \\ \sigma'_x & \sigma'_y & \sigma'_z & 2\tau_{yz} & 2\tau_{zx} & 2\tau_{xy} \\ 0 & 0 & 0 & 0 & 0 & 0 \\ 0 & 0 & 0 & 0 & 0 & 0 \\ 0 & 0 & 0 & 0 & 0 & 0 \end{bmatrix}$$

$$\mathbf{a}_1\mathbf{a}_3^T = \mathbf{M}_8 = \begin{bmatrix} A & B & C & D & E & F \\ A & B & C & D & E & F \\ A & B & C & D & E & F \\ 0 & 0 & 0 & 0 & 0 & 0 \\ 0 & 0 & 0 & 0 & 0 & 0 \\ 0 & 0 & 0 & 0 & 0 & 0 \end{bmatrix}$$

$$\mathbf{a}_2\mathbf{a}_1^T = \frac{1}{2\sqrt{J_2'}}\mathbf{M}_7^T$$

$$\mathbf{a}_3\mathbf{a}_1^T = \mathbf{M}_8^T$$

$$\mathbf{a}_3\mathbf{a}_2^T = \frac{1}{2\sqrt{J_2'}}\mathbf{M}_6^T$$

$$\mathbf{b}\mathbf{a}_1^T = -\frac{\sqrt{3}}{2J_2'^{9/2}\cos 3\theta}\mathbf{M}_8^T + \frac{\tan 3\theta}{2J_2'^4}\mathbf{M}_7^T$$

$$\mathbf{b}\mathbf{a}_2^T = -\frac{\sqrt{3}}{4J_2'^5\cos 3\theta}\mathbf{M}_6^T + \frac{\tan 3\theta}{4J_2'^{9/2}}\mathbf{M}_2$$

$$\mathbf{b}\mathbf{a}_3^T = -\frac{\sqrt{3}}{2J_2'^{9/2}\cos 3\theta}\mathbf{M}_5 + \frac{\tan 3\theta}{2J_2'^4}\mathbf{M}_6$$

The term $\frac{\partial \mathbf{a}^T}{\partial \boldsymbol{\sigma}}$ of equation 3.14 now can written in term of the stresses as

$$\begin{aligned}\frac{\partial \mathbf{a}^T}{\partial \boldsymbol{\sigma}} &= \frac{c_2}{2\sqrt{J_2'}}\mathbf{M}_1 - \frac{c_2}{4J_2^{3/2}}\mathbf{M}_2 + c_3\mathbf{M}_3 \\ &+ f_1\mathbf{M}_4 + \frac{f_2}{2\sqrt{J_2'}}\mathbf{M}_7^T + f_3\mathbf{b}\mathbf{a}_1^T \\ &+ \frac{f_4}{2\sqrt{J_2'}}\mathbf{M}_7 + \frac{f_5}{4J_2'}\mathbf{M}_2 + f_6\mathbf{b}\mathbf{a}_2^T \\ &+ f_7\mathbf{M}_8 + \frac{f_8}{2\sqrt{J_2'}}\mathbf{M}_6 + f_9\mathbf{b}\mathbf{a}_3^T \end{aligned} \tag{3.16}$$

in which f_i, $i = 1, 9$ are the derivatives of c_j, $j = 1, 3$ with respect to J_1, $J_2^{'1/2}$, and θ respectively.

The other term of $\mathbf{H}^n$, that is $\mathbf{a}\mathbf{a}^T$, gives;

$$\begin{aligned}\mathbf{a}\mathbf{a}^T &= c_1^2\mathbf{a}_1\mathbf{a}_1^T + c_2^2\mathbf{a}_2\mathbf{a}_2^T + c_3^2\mathbf{a}_3\mathbf{a}_3^T \\ &\quad + c_1c_2\mathbf{a}_1\mathbf{a}_2^T + c_1c_3\mathbf{a}_1\mathbf{a}_3^T + c_1c_2\mathbf{a}_2\mathbf{a}_1^T \\ &\quad + c_2c_3\mathbf{a}_2\mathbf{a}_3^T + c_1c_3\mathbf{a}_3\mathbf{a}_1^T + c_2c_3\mathbf{a}_3\mathbf{a}_2^T \end{aligned} \tag{3.17}$$

Using the other terms of $\mathbf{a}_i\mathbf{a}_j^T$ as described previously, equation 3.17 can be expressed as

$$\begin{aligned}\mathbf{a}\mathbf{a}^T &= c_1^2\mathbf{M}_4 + \frac{c_2^2}{4\sqrt{J_2'}}\mathbf{M}_2 \\ &\quad + c_3^2\mathbf{M}_5 + \frac{c_1c_2}{2\sqrt{J_2'}}(\mathbf{M}_7 + \mathbf{M}_7^T) \\ &\quad + c_1c_3(\mathbf{M}_8 + \mathbf{M}_8^T) + \frac{c_2c_3}{2\sqrt{J_2'}}(\mathbf{M}_6 + \mathbf{M}_6^T) \end{aligned} \tag{3.18}$$

The terms that depend on the assumed yield function are the constant c_i and its derivatives f_j since matrices $\mathbf{M}$ do not depend on the yield function. The following sections will evaluate the constants c_i and f_j.

3.1.2 Alternative form of the yield criteria

In order to have the yield criterion independent of axes rotation, it should be in a function of the stress invariants.

For $\sigma_1 \geq \sigma_2 \geq \sigma_3$, we have:

- Tresca

$$\sigma_1 - \sigma_3 = \tau(k)$$

- von-Mises

$$\sqrt{J_2'} = k(k)$$

$$J_2' = \sigma_{ij}'\,\sigma_{ij}' = \frac{1}{6}\left[(\sigma_1-\sigma_2)^2+(\sigma_2-\sigma_3)^2+(\sigma_3-\sigma_1)^2\right]$$
$$= \frac{1}{2}\left[\sigma_x'^2+\sigma_y'^2+\sigma_z'^2\right]+\tau_{xy}^2+\tau_{yz}^2+\tau_{xz}^2$$

- Mohr-Coulomb

$$\tau = c-\sigma_n\,\tan\phi$$

Expressing τ and σ_n in terms of σ_1 , σ_2 and σ_3 , we obtain

$$-\frac{1}{2}(\sigma_1-\sigma_3)\cos\phi = c-\left(\frac{\sigma_1+\sigma_3}{2}-\frac{\sigma_1-\sigma_3}{2}\sin\phi\right)\tan\phi$$

or

$$(\sigma_1-\sigma_3) = 2\,c\,\cos\phi-(\sigma_1+\sigma_3)\sin\phi$$

- Drucker-Prager

$$\alpha\,J_1+(J_2')^{1/2} = k'$$

where

$$\alpha = \frac{2\,\sin\phi}{\sqrt{3}(3-\sin\phi)}$$

$$k' = \frac{6\,c\,\cos\phi}{\sqrt{3}(3-\sin\phi)}$$

Noticing that

$$\begin{Bmatrix} \sigma_1 \\ \\ \sigma_2 \\ \\ \sigma_3 \end{Bmatrix} = \frac{2\sqrt{J_2'}}{\sqrt{3}} \begin{Bmatrix} \sin(\theta + \frac{2\pi}{3}) \\ \\ \sin\theta \\ \\ \sin(\theta + \frac{4\pi}{3}) \end{Bmatrix} + \frac{J_1}{3} \begin{Bmatrix} 1 \\ \\ 1 \\ \\ 1 \end{Bmatrix}.$$

the above yield surfaces can be expressed in terms of the stress invariants as follows:

- Tresca

$$\frac{2\sqrt{J_2'}}{\sqrt{3}} \left[\sin\left(\theta + \frac{2\pi}{3}\right) - \sin\left(\theta + \frac{4\pi}{3}\right) \right] = \tau(k)$$

or

$$2\left(J_2'\right)^{1/2} \cos\theta = \tau(k) = \sigma_y(k)$$

- von-Mises

$$\sqrt{3}\sqrt{J_2'} \;=\; \sigma_y(k)$$

- Mohr-Coulomb

$$\frac{1}{3} J_1 \sin\phi + \sqrt{J_2'} \left(\cos\theta - \frac{1}{\sqrt{3}} \sin\theta \sin\phi \right) = c\cos\phi$$

- Drucker-Prager

$$\alpha\, J_1 + \left(J_2'\right)^{1/2} \;=\; k'$$

3.1.3 Constants c_i

In the various yield criteria, constants c_i of equation 3.11, 3.12, and 3.13 have the following values:

- Tresca

$$
\begin{aligned}
c_1 &= 0 \\
c_2 &= 2\ \cos\theta\,(1+\tan\theta\ \tan 3\theta) \\
c_3 &= \frac{\sqrt{3}}{J_2'}\,\frac{\sin\theta}{\cos 3\theta}
\end{aligned}
$$

- von-Mises

$$
\begin{aligned}
c_1 &= 0 \\
c_2 &= \sqrt{3} \\
c_3 &= 0
\end{aligned}
$$

- Mohr-Coulomb

$$
\begin{aligned}
c_1 &= \frac{1}{3}\sin\phi \\
c_2 &= \cos\theta\left[(1+\tan\theta\ \tan 3\theta)+\frac{\sin\phi}{\sqrt{3}}\,(\tan 3\theta-\tan\theta)\right] \\
c_3 &= \left[\sqrt{3}\sin\theta+\cos\theta\sin\phi\right]\frac{\sqrt{3}}{2\sqrt{J_2'}\cos 3\theta}
\end{aligned}
$$

- Drucker-Prager

$$
\begin{aligned}
c_1 &= \alpha \\
c_2 &= 1.0 \\
c_3 &= 0.0
\end{aligned}
$$

3.1.4 Constants f_j

The constants f_j, $j = 1,9$ are obtained by differentiating c_i, $i = 1,3$ which may be a function of stress invariants and/or the direction of principal stresses.

- Tresca

$$f_1 = f_2 = f_3 = f_4 = f_5 = f_7 = 0$$

$$\begin{aligned} f_6 &= -2\sin\theta(1+\tan\theta\tan 3\theta) + \frac{2\tan 3\theta}{\cos\theta} + \frac{6\sin\theta}{\cos^2 3\theta} \\ f_8 &= -\frac{2\sqrt{3}}{(J_2')^{3/2}}\frac{\sin\theta}{\cos 3\theta} \\ f_9 &= \frac{\sqrt{3}}{J_2'}\left(\frac{\cos\theta\cos 3\theta + 3\sin\theta\sin 3\theta}{\cos^2 3\theta}\right) \end{aligned}$$

- von-Mises

$$f_1 = f_2 = f_3 = f_4 = f_5 = f_6 = f_7 = f_8 = f_9 = 0$$

- Mohr-Coulomb

$$f_1 = f_2 = f_3 = f_4 = f_5 = f_7 = 0$$

$$\begin{aligned} f_6 &= \cos\theta\left[\frac{3\tan\theta}{\cos^2 3\theta} + \frac{\tan 3\theta}{\cos^2\theta} + \frac{\sin\phi}{\sqrt{3}}\left(\frac{3}{\cos^2 3\theta} - \frac{1}{\cos^2\theta}\right)\right] \\ &\quad - \sin\theta\left[(1+\tan\theta\tan 3\theta) + \frac{\sin\phi}{\sqrt{3}}(\tan 3\theta - \tan\theta)\right] \end{aligned}$$

$$\begin{aligned} f_8 &= (J_2')^{-3/2}\left(\frac{\sqrt{3}\sin\theta + \cos\theta\sin\phi}{\cos 3\theta}\right) \\ f_9 &= \frac{3\tan 3\theta}{\cos 3\theta}\left(\sqrt{3}\cos\theta - \sin\theta\sin\phi + \sqrt{3}\sin\theta + \cos\theta\sin\phi\right) \end{aligned}$$

- Drucker-Prager

$$f_1 = f_2 = f_3 = f_4 = f_5 = f_6 = f_7 = f_8 = f_9 = 0$$

3.2 Development of mining excavation process

The excavation is simulated by assigning very small values to the modulus of elasticity, stress, strain, and load for the element/s to be removed. Consider the equilibrium equation at time station t_{n+1} of the form

$$\Psi^{n+1} = \mathbf{F}_{int}^{n+1} - \mathbf{F}_{ext}^{n+1}$$

where Ψ^{n+1} is the out-of-balance force vector, $\mathbf{F}_{int}^{n+1}$ is the internal force vector and $\mathbf{F}_{ext}^{n+1}$ is the external force vector. The internal and external force vector for the whole domain can be written as;

$$\mathbf{F}_{int}^{n+1} = \int_{\Gamma} \mathbf{B}^T \boldsymbol{\sigma}^{n+1} d\Gamma$$

$$\mathbf{F}_{ext}^{n+1} = \int_{\Gamma} \mathbf{N}^T \mathbf{q} d\Gamma$$

Vector $\mathbf{q}$ is the traction force, and other forces can be included in the external force vector without difficulty.

In the excavation process, the out-of-balance vector Ψ^{n+1} results from the subtraction of the following contribution of the eliminated element/s from the respective global force vector:

$$\mathbf{F}_{int}^{excav} = \sum_{i=1}^{n} \int_{\Omega} \mathbf{B}^T \boldsymbol{\sigma}^{n+1} d\Omega$$

$$\mathbf{F}_{ext}^{excav} = \sum_{i=1}^{n} \int_{\Omega} \mathbf{N}^T \mathbf{q} d\Omega$$

where n is the number of eliminated elements.

The overlay models are created by placing several layers having exactly the same in-plane geometrical properties one on top of the other. This means that an element of an overlay model has the same shape, coordinates, boundary conditions, and

element numbering sequence on every layers. However, its material properties and its thickness may be different. Due to this features, element removal in the overlay model is possible, the main step being as follows:
Consider n_l number of layers having n_e number of elements.

- The number of element on each layer is

$$n_e^1 = \frac{n_e}{n_l}$$

- The element numbers to be removed are

$$i_e = i_e^1 + i_l - 1 \qquad i_l = 1, n_l$$

  where i_e^1 is the selected element number to be removed on the first layer and i_l is the layer number.

- Assign new material property numbers to the removed elements to differentiate from the unremoved elements
- Set very low values of Young's moduli to the removed elements
- For the removed elements assign zero values to the following quantities;
  - element loads on each node
  - element stresses on each Gauss point
  - element strain and strain rate on each Gauss point
- Assembly the global stiffness matrix
- Assembly the global load vector
- Solve the $\mathbf{Kd} = \mathbf{f}$ equation

3.3 Program features and organization

The finite element capabilities of the program are self explanatory, the interactive and graphics features of the program being as follows:

- The analysis can be paused any time step during the process.
- The finite element discretization is displayed on the screen.
- A maximum of 50 elements can be eliminated at any arbitrary time station and the new mesh is automatically displayed.
- The loading including its numerical value can be displayed.
- The element number, node number, material number, and boundary conditions can be displayed.
- Zoom capability is provided.
- Deformed mesh on top of undeformed mesh is automatically displayed.
- The coordinates and displacements of a selected node can be displayed one at a time.
- Yielded Gauss points can be displayed.
- Stresses, including the extremes and direction, and viscoplastic strain is displayed with two different colors for tension and compression.
- The value of Δt can be modified at any time station.
- History of stresses, viscoplastic strains, displacements, and room closures can be displayed using cuvre plot or contour line or colored shades.

The program is composed of 88 subroutines and it is written in Fortran. The main program and subroutines that perform finite element analysis are organized as shown on the following flow chart.

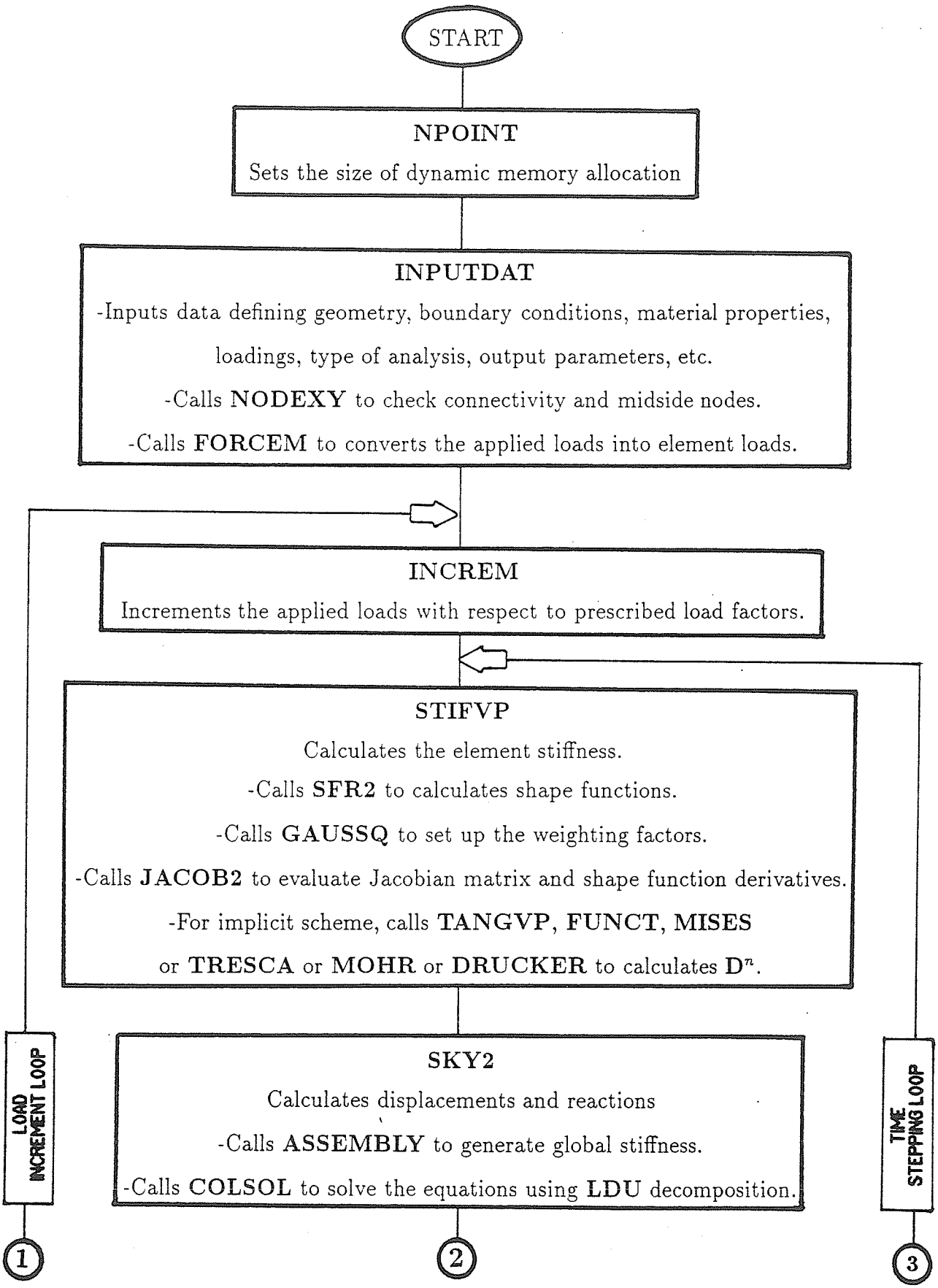
START
NPOINT
Sets the size of dynamic memory allocation
INPUTDAT
-Inputs data defining geometry, boundary conditions, material properties,
loadings, type of analysis, output parameters, etc.
-Calls NODEXY to check connectivity and midside nodes.
-Calls FORCEM to converts the applied loads into element loads.
INCREM
Increments the applied loads with respect to prescribed load factors.
STIFVP
Calculates the element stiffness.
-Calls SFR2 to calculates shape functions.
-Calls GAUSSQ to set up the weighting factors.
-Calls JACOB2 to evaluate Jacobian matrix and shape function derivatives.
-For implicit scheme, calls TANGVP, FUNCT, MISES
or TRESCA or MOHR or DRUCKER to calculates D^n.
SKY2
Calculates displacements and reactions
-Calls ASSEMBLY to generate global stiffness.
-Calls COLSOL to solve the equations using LDU decomposition.
LOAD INCREMENT LOOP
TIME STEPPING LOOP
1
2
3

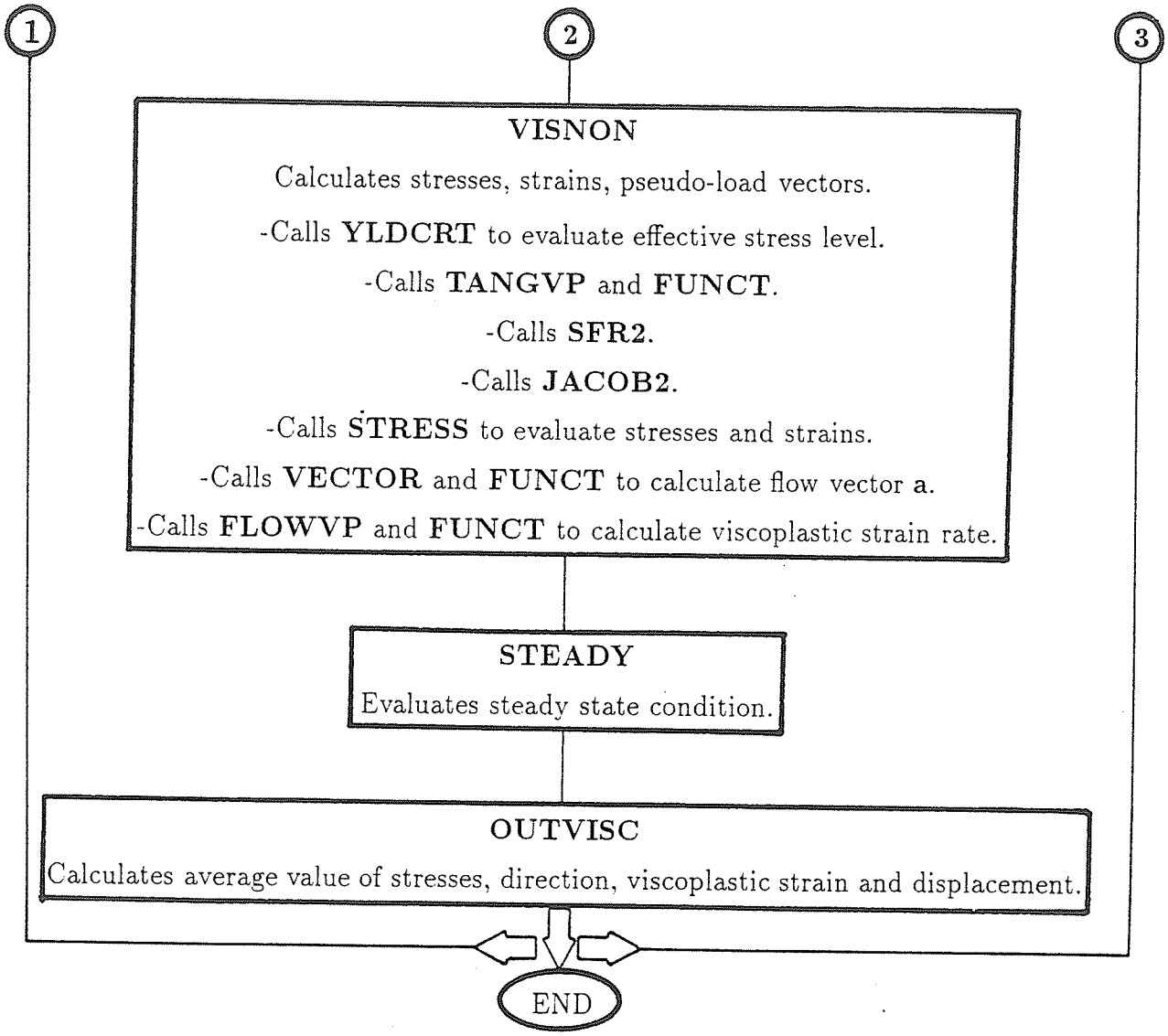
1
2
3
VISNON
Calculates stresses, strains, pseudo-load vectors.
-Calls YLDCRT to evaluate effective stress level.
-Calls TANGVP and FUNCT.
-Calls SFR2.
-Calls JACOB2.
-Calls STRESS to evaluate stresses and strains.
-Calls VECTOR and FUNCT to calculate flow vector a.
-Calls FLOWVP and FUNCT to calculate viscoplastic strain rate.
STEADY
Evaluates steady state condition.
OUTVISC
Calculates average value of stresses, direction, viscoplastic strain and displacement.
END

Chapter 4

Case Studies

4.1 Introduction

This chapter has three components. The first section validates the numerous capabilities of the program with reference to a semi-analytical solution of the simple uniaxial case. This validation is necessary as it not only allows us to tackle the modelling process with a certain degree of confidence, but also it gives us a feeling about the accuracy, stability of the numerical solution, and sensibility of the parameters involved. Section 4.3 studies the numerical simulation of the experimental creep tests conducted in reference [19]. After this stage field modelling is ready to commence. Section 4.4 presents a numerical simulation of the potash mining process and a comparison of the results with a collection of field measurement data.

4.2 Program verification

Before being applied to complex case studies, a finite element program should be validated for the correctness of the result with refernce to a semi-analytical solution based on finite difference. This is normally accomplished through comparison with a simpler, predictable example. For this program a short column fixed in the x and y directions at one end and subjected to uniaxial uniform load on the other end was chosen as the test-problem with the model characteristics assumed to be:

- Model size 1 unit width, 2 unit height, and 1 unit cross section area

- Plane stress analysis
- Four linear element on each layer
- Modulus of elasticity $E = 30000$
- Poisson's ratio $\nu = 0.30$
- Cohesion $c = 5.0$
- Hardening parameter $H' = 5000$
- Angle of internal friction $\phi = 0$
- Fluidity parameter $\gamma = 0.0001$
- Time increment $\Delta t = 0.1$
- Flow function $\frac{F-F_o}{F_o}$
- Uniform distributed load $w = 15$

The semi-analytical solution is obtained by setting up the one-dimensional governing equations for the cases of Mohr-Coulomb and Drucker-Prager yield functions. The non-linear differential equations are solved using the Euler forward finite difference scheme.

For a uniaxial loading, the stress invariants and yield functions are first evaluated and the governing equation is subsequently established.

- stress invariants

$$\begin{array}{ll} J_1 = \sigma & J_1' = 0 \\ J_2 = 0 & J_2' = \frac{1}{3}\sigma^2 \\ J_3 = 0 & J_3' = \frac{2}{27}\sigma^3 \end{array}$$

- yield function

1. Mohr-Coulomb: $F = \frac{1}{3}\sqrt{3}\sigma$ and $\sigma_y = c$

2. Drucker-Prager: $F = \frac{1}{3}\sqrt{3}\sigma$ and $\sigma_y = \frac{2}{3}c\sqrt{3}$

- strain and displacement

  $\dot{\epsilon} = \dot{\epsilon}_e + \dot{\epsilon}_{vp}$

  $\dot{\epsilon} = \dot{\epsilon}_e + \gamma < \Phi(F) > \frac{\partial F}{\partial \sigma}$

  $\dot{\epsilon} = \frac{\dot{\sigma}}{E} + \frac{1}{3}\sqrt{3}\gamma \left[\frac{\frac{1}{3}\sqrt{3} - (\sigma_y + H'\epsilon_{vp})}{\sigma_y + H'\epsilon_{vp}}\right]$

  A constant $\sigma = \sigma_a$ gives $\dot{\sigma} = 0$ and the differential equation is found to be

$$\dot{\epsilon}(\sigma_y + H'\epsilon_{vp}) + H'\dot{\epsilon}\epsilon + \gamma H'\epsilon = \gamma \left[\sigma_a(\frac{1}{3}\sqrt{3} + \frac{H'}{E}) - \sigma_y\right] \qquad (4.1)$$

  Using the forward finite difference scheme of the form

  $\epsilon_{n+1} = \epsilon_n + \dot{\epsilon}_n \Delta t$

  or

  $\dot{\epsilon}_n = \frac{\epsilon_{n+1} - \epsilon_n}{\Delta t}$

  the differential equation can be written in the form

  $A\dot{\epsilon}_n + H'\dot{\epsilon}_n\epsilon_n + \gamma H'\epsilon_n = B$, and

  the time-marching of the solution is performed via:

  $\epsilon_{n+1} = \frac{B + \epsilon_n(C - \gamma H')}{C}$

  where,

  $A = \sigma_y + H'\frac{\sigma_a}{E}$

  $B = \gamma \left[\sigma_a(\frac{1}{3}\sqrt{3} + \frac{H'}{E}) - \sigma_y\right]$

  $C = \frac{A + H'\epsilon_n}{\Delta t}$

  Finally, the displacement is calculated by multiplying strain by the length of the model.

  The time increment used in calculation is 0.1 unit.

The following investigations were conducted and compared to the semi-analytical solution:

- test-case 1

1. One overlay of elasto-viscoplastic plane stress model
2. Mohr-Coulomb yield criterion
3. Solution strategies are:
   - Explicit-Initial Stiffness
   - Explicit-Tangential Stiffness
   - Implicit-Initial Stiffness
   - Implicit-Tangential Stiffness

- test-case 2
  The same configuration as test-case 1 except the Drucker-Prager yield criterion was used.

- test-case 3
  Comparison of test-case1 and test-case2.

- test-case 4
  A two-overlay model with thicknesses of 0.7 and 0.3 was used. The individual configurations of each layer are the same as those of test-case 1. This test problem is designed to validate the overlay model.

The displacements of the top-center of column from test-case 1, test-case 2, test-case 3, and test-case 4 are shown in Figure 4.1, Figure 4.2, Figure 4.3, and Figure 4.4 respectively.

It can be concluded that both the implicit and explicit time integration algorithms yield the same result as the theoretical solution and the multilayer algorithm result reproduce the single layer model. Thus, the program is considered to be ready for further application.

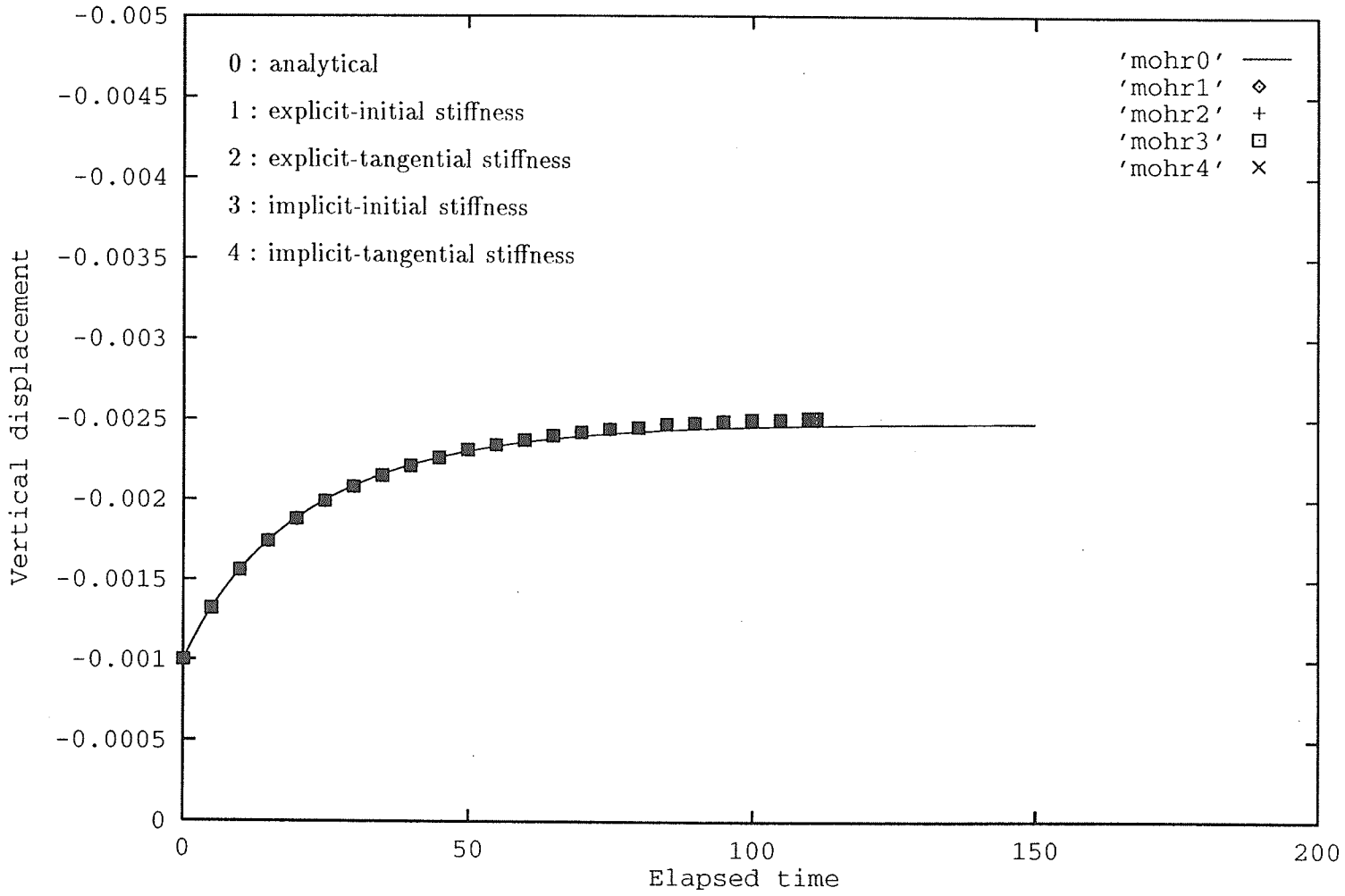

Figure 4.1: Test-case 1: displacement vs time

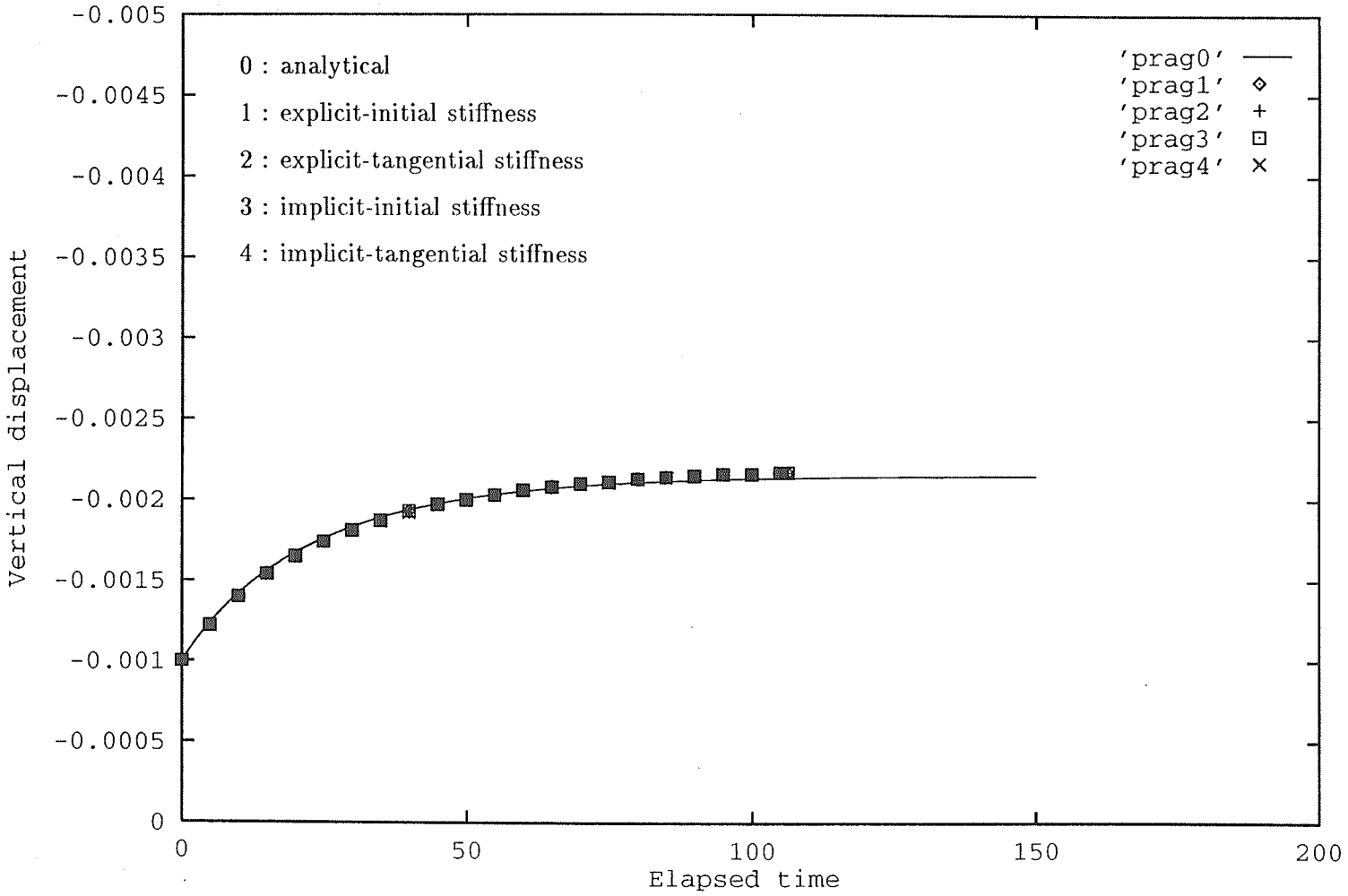

Figure 4.2: Test-case 2: displacement vs time

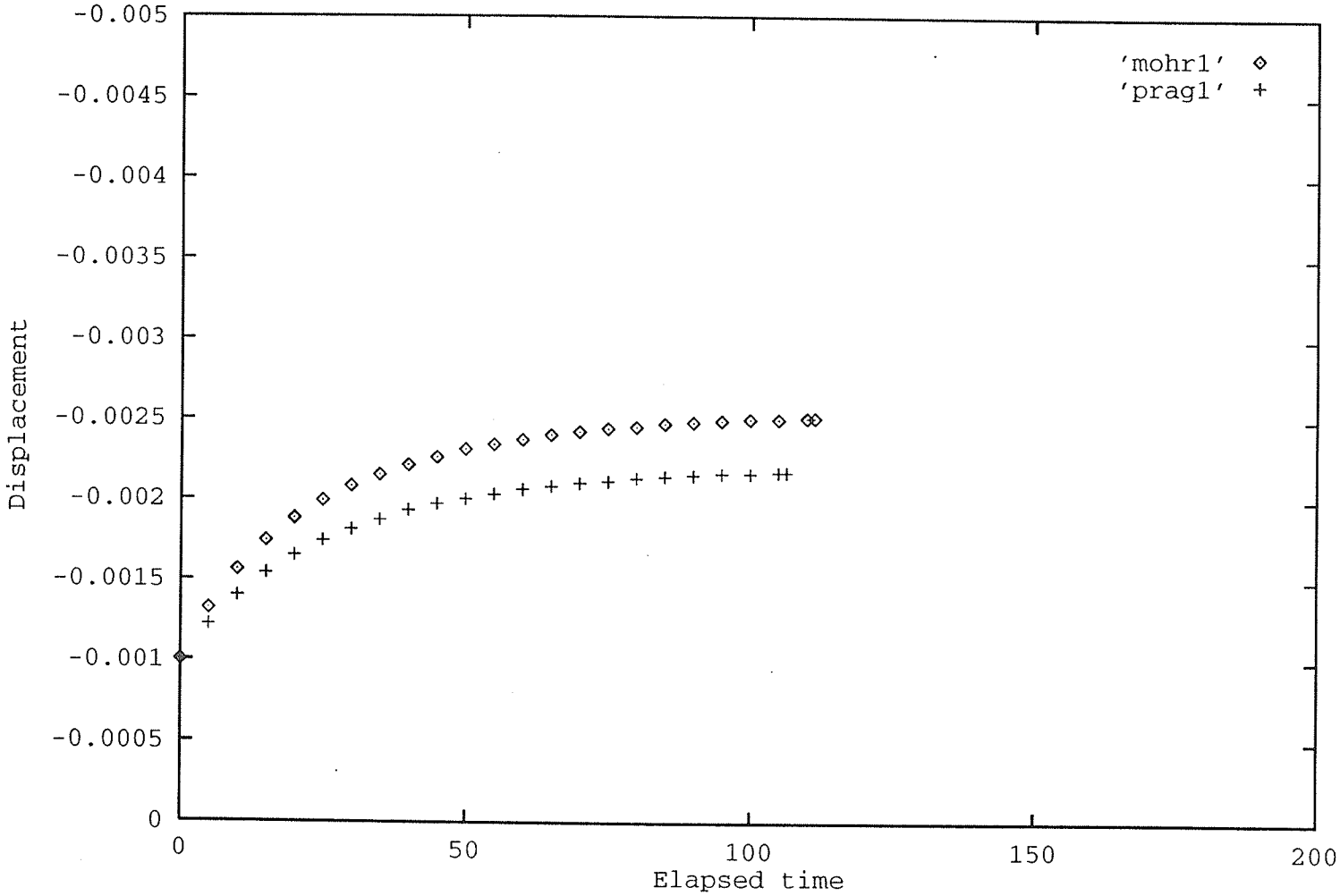

Figure 4.3: Test-case 3: displacement vs time

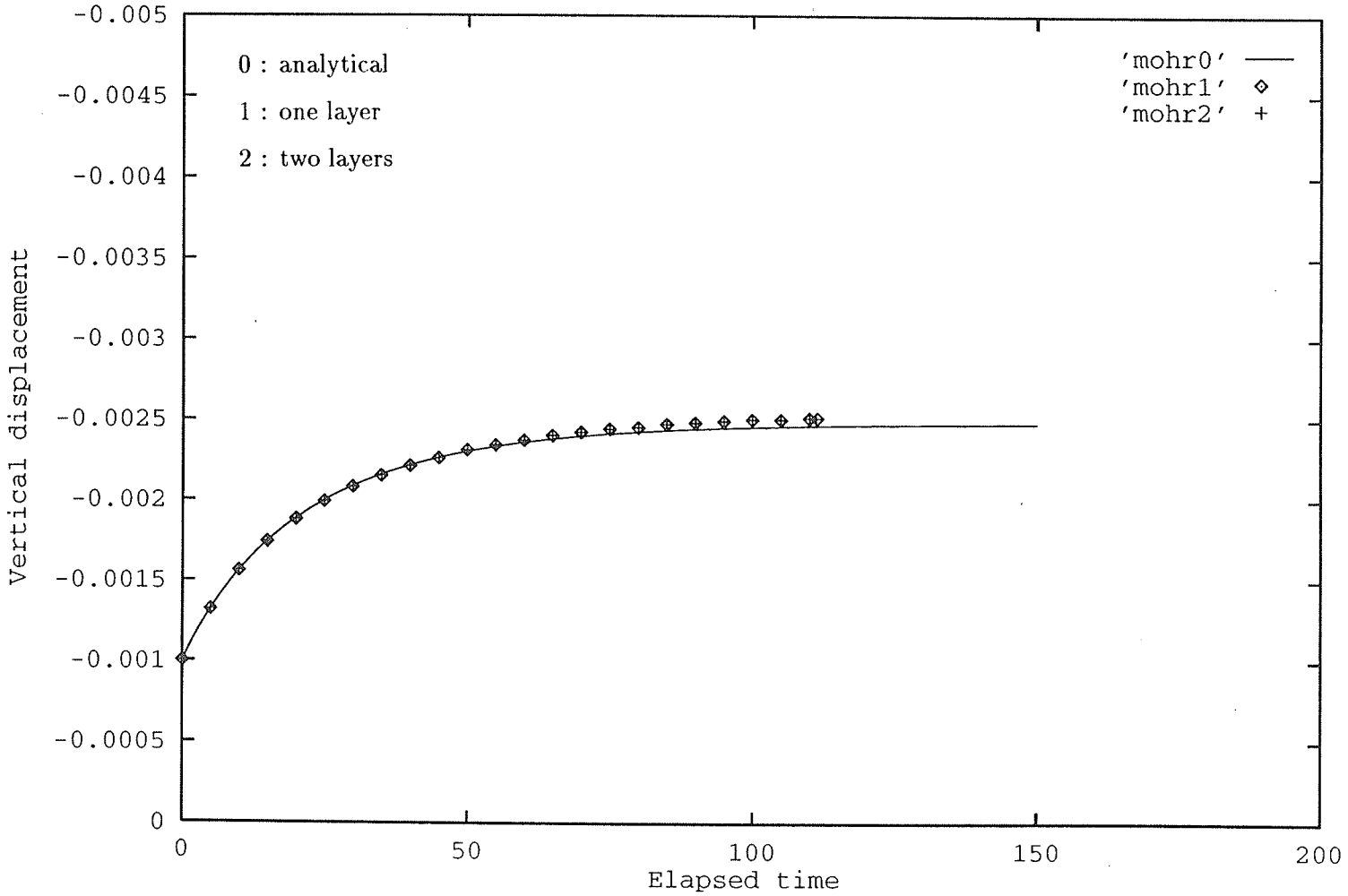

Figure 4.4: Test-case 4: displacement vs time

4.3 Case study 1 - Simulation of uniaxial creep test of Lanigan potash

4.3.1 Introduction

A series of creep tests of Esterhazy (Rocanville) and the Patience Lake (Lanigan) types of potash salt rock was conducted in order to investigated its time-dependent behaviour under various constant uniaxial compressive loads [19], [20]. The specimens were cored from Rocanville and Lanigan mines which operate at the approximate depth of 1000 m.

In this study, simulation is conducted only on four Patience Lake (Lanigan) potash specimens. Both axial and lateral strain creep were recorded over a two month period to six month period. The uniaxial compressive loads are 7 MPa, 9MPa, 11 MPa, and 13 MPa. Cylindrical specimens with the average sizes of 53.50 mm in diameter and 110.00 mm in height were used for the analysis.

4.3.2 Objective

The objective of the study is to design a model which correlates both the axial and lateral creep strain of Lanigan potash which are obtained experimentally and reported in reference [19] and [20].

4.3.3 Developement of the model

The selected rheological model and its properties used in this simulation were obtained by trial. Since the specimens are symmetric in both geometry and loading with respect to all axes, axisymmetric analyses were used. The model is discretized into two overlays with two quadratic elements on each overlay. The discretization and rheological arrangement of the model are shown in Figure 4.5. The tangential stiffness method and implicit time integration scheme as well as Mohr -Coulomb yield criterion were used during the analyses. Material properties of the model were

as follow:

- Overlay 1

  1. Overlay thickness $t = 0.5$
  2. Modulus of elasticity $E = 4.7\ GPa$
  3. Poisson's ratio $\nu = 0.20$
  4. Cohesion $c = 0.1\ MPa$
  5. Hardening parameter $H' = 6000$
  6. Angle of internal friction $\phi = 60\ degree$
  7. Fluidity parameter $\gamma = 1.0x10^{-5}$
  8. Time increment $\Delta t = 1.0\ day$
  9. Flow function $10^{-5}\left(\frac{F}{F_o}\right)^{5.9}$

- Overlay 2

  1. Overlay thickness $t = 0.5$
  2. Modulus of elasticity $E = 5.0\ GPa$
  3. Poisson's ratio $\nu = 0.20$
  4. Cohesion $c = 0\ MPa$
  5. Hardening parameter $H' = 0$
  6. Angle of internal friction $\phi = 58\ degree$
  7. Fluidity parameter $\gamma = 1.0x10^{-4}$
  8. Time increment $\Delta t = 1.0\ day$
  9. Flow function $10^{-5}\left(\frac{F}{F_o}\right)^{5.0}$

4.3.4 Results

The computed axial and lateral strains at the top-center of the model are indicated in Figure 4.6 and Figure 4.7 respectively, which also show the experimental creep curves. In Figure 4.6, curves a7 through a13 represent the axial microstrains computed analytically, while curves o7 through o13 represent the experimental counterpart for the loadings of 7, 9, 11, and 13 MPa respectively. Similar observation is made for the lateral strains in Figure 4.7.

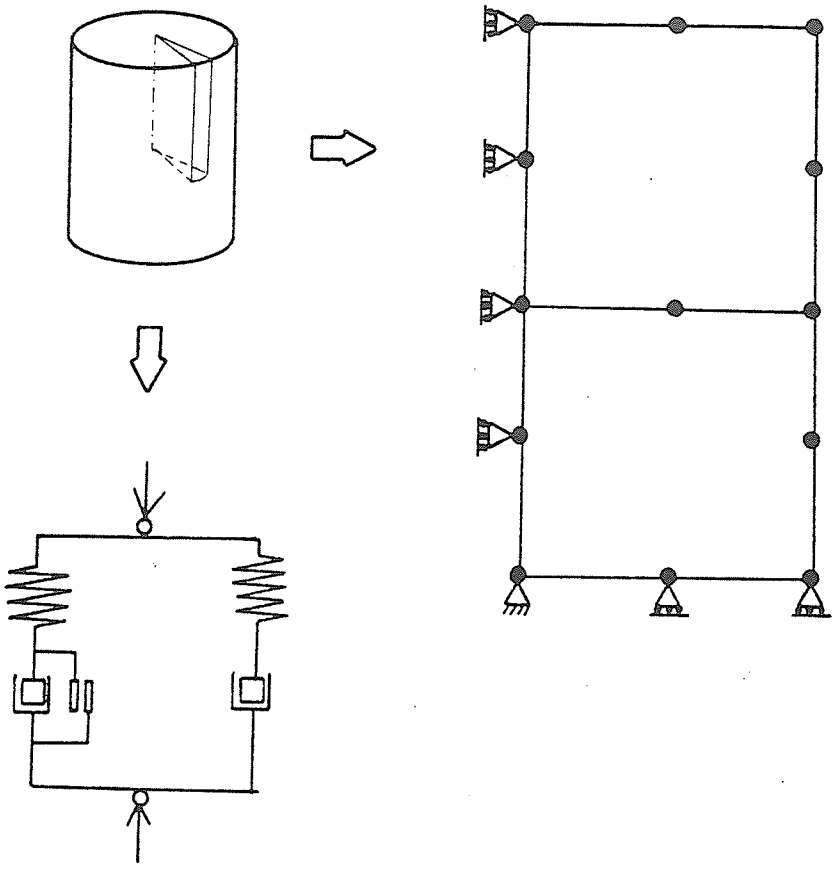

Figure 4.5: Model characteristics of the specimen

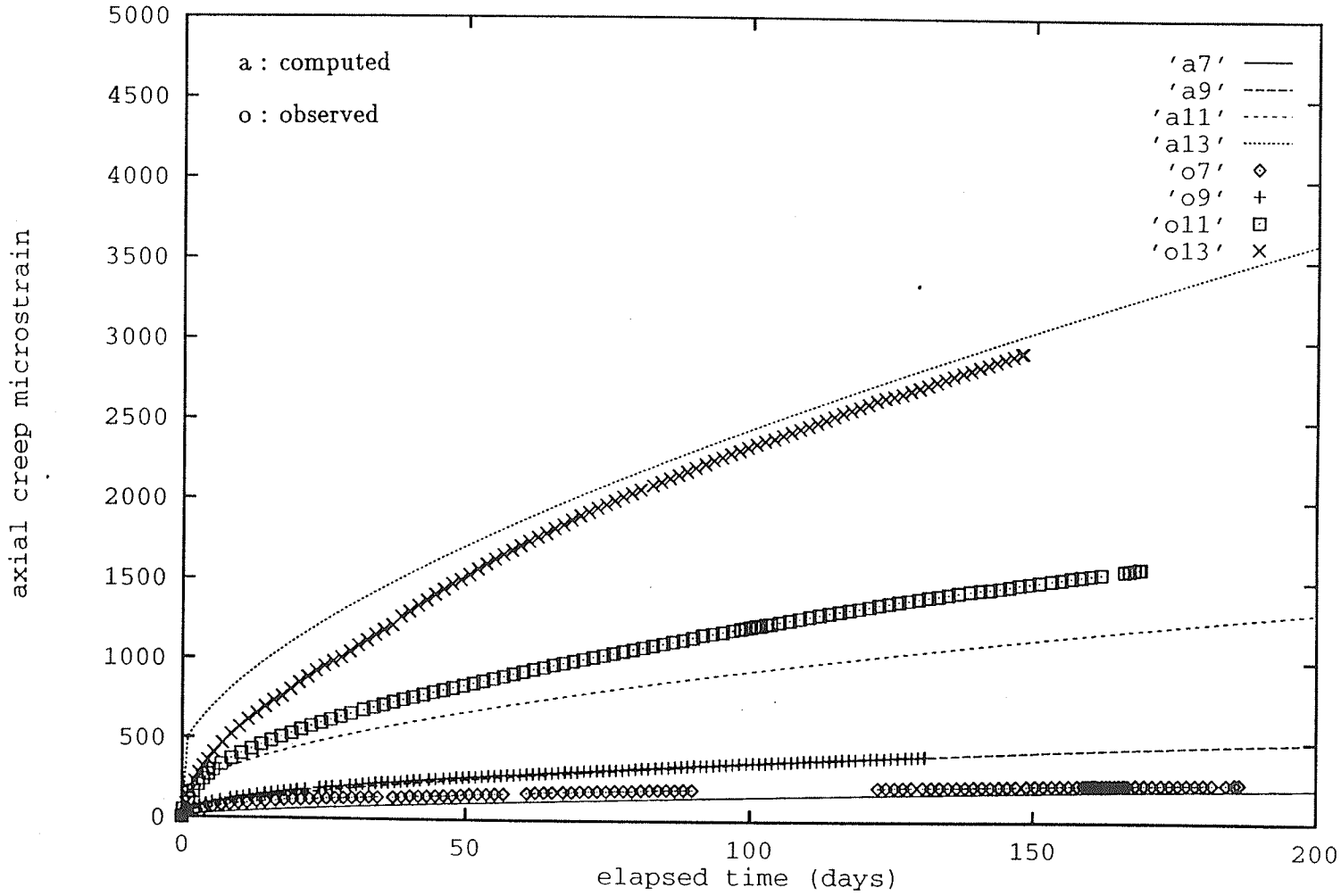

Figure 4.6: Axial creep strain.

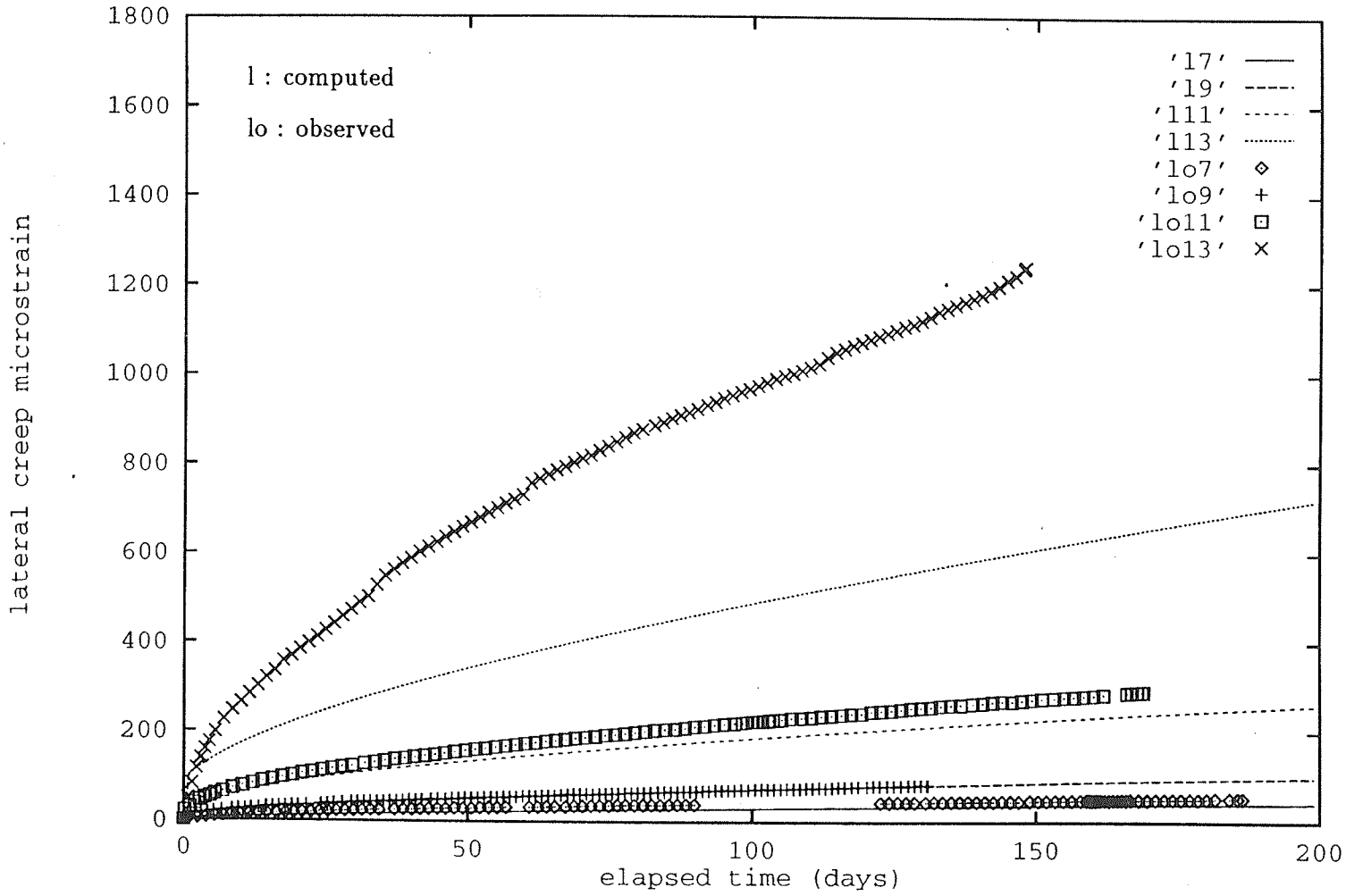

Figure 4.7: Lateral creep strain.

4.3.5 Discussion of results

Despite the deviation of 11 MPa and 13 MPa overall computed lateral creep strain, the response of the model can be considered to be in good agreement with the observed response. This deviation is mainly caused by assosiated micro-cracking [19], [20] which is not incorporated in the model.

The material properties used in the model are reasonable, however, the modulus of elasticity is not in agreement with the experimental results. The modulus of elasticity of 4.85 GPa used in the model is out of the range of 15.0 GPa to 30.0 GPa found experimentally in reference [20]. However, it is close to the value of 4.29 GPa given by Potash Corporation of Saskatchewan Inc. [25]. At this stage, it is important to notice the difference between the instantneous modulus of elasticity and the long term modulus of elasticity. The low value of E is inevitable in correlating the analytical solution with the experimental results.

After six months of continuously controled creep testing, the steady state response is not achieved, and the subsequent tertiary response is not reported. A complete response which traces the primary, steady state, and tertiary state can be achieved with a piece-wise linear hardening and softening of the yield surface. In the absence of experimental evidence which reaches the steady state and tertiary stages the following investigation will be limited to modelling linear hardening.

4.4 Case study 2 - Simulation of potash mining process

4.4.1 Introduction

This study was carried out based on the work that had been done in reference [26]. The main scope of that work was the collection and evaluation of field data around potash excavations located about 1100 m below ground surface. There are five openings, four of which are 5.5 m wide by 3.35 m high rooms and one 7.0 m wide

by 3.35 m high room. The rooms are excavated in a certain sequence and these rooms are separated by nominal 6.7 m pillars. The opening or room number and the excavation completion dates are shown in Figure 4.8.

Data was collected in rooms 2103, 2104, and 2105 and covers the following major aspects:

- Vertical and horizontal closure histories, which were obtained by drum recorders.
- Strain history of floor and pillar, obtained by borehole extensometers.
- Stress history corresponding to extensometer location, obtained by hydraulic pressure gauges.

Unfortunately, mechanical properties and geological cross-sections of the rock are not available for this report.

4.4.2 Objective

A great number of questions can be raised with respect to this mining process. This study attempts to simulate the displacement or closure behaviour of rooms and vertical stress history of pillars and wall in correlation with the mining process. Explicitly, this study tries to simulate two aspects which can be implied from the field observation; these are

1. The closing or possible failure sequence of the rooms begins from the outer room to the inner room.
2. Reloading effect is produced while cutting the adjacent room.

4.4.3 Developement of the model

The size of the model is 68.35 m high by 115.80 m wide and it is divided into 600 four-noded elements. The model is supported by rollers on the vertical sides and by hinges on the bottom. The model is assumed to have a geological cross-section

as in Figure 4.9 having an average unit weight of 0.0022 kg/cm^2, as taken from reference [25]. While Dawson Bay and the Red Beds formations are assumed to behave elastically, halite and potash are considered elasto-viscoplastic having the same material properties. Clay seam above the potash layer is neglected. The finite element mesh is shown in Figure 4.10. Plane strain conditions, Mohr-Coulomb yield function, and one layer of elasto-viscoplastic model are adopted with the following characteristics:

1. **Dawson Bay Formation**

   - Modulus of elasticity $E = 340,000\ kg/cm^2$
   - Cohesion $c = 40\ kg/cm^2$
   - Angle of internal friction $\phi = 70\ degree$

2. **Red Bed Formation**

   - Modulus of elasticity $E = 250,000\ kg/cm^2$
   - Cohesion $c = 40\ kg/cm^2$
   - Angle of internal friction $\phi = 60\ degree$

3. **Halite and Potash**

   - Modulus of elasticity $E = 230,000\ kg/cm^2$
   - Unit weight $\mu = 0.0022\ kg/cm^2$
   - Poisson's ratio $\nu = 0.20$
   - Cohesion $c = 2.5\ kg/cm^2$
   - Angle of internal friction $\phi = 0 degree$
   - Hardening parameter $H' = 3000$
   - Fluidity parameter $\gamma = 5.0x10^{-5}$
   - Initial time increment $\Delta t_o = 5\ days$

- Flow function $\frac{F-F_o}{F_o}$
- Mining depth $h = 1045\ m$
- uniform vertical distributed load $= \mu h = 230\ kg/cm^2$

The model is first allowed to deform elastically in order to simulate the state of *virgin stresses*. Since field measurements are conducted after the completion of the excavation, the rooms are then assumed to be excavated instantenously according to the following sequence:

1. Room 2105 is excavated at day 0.
2. Room 2101 is excavated at day 25.
3. Room 2104 is excavated at day 95.
4. Room 2102 is excavated at day 105.
5. Room 2103 is excavated at day 120.

4.4.4 Results

The simulated *virgin stresses* are 230 kg/cm^2 vertical stress and 60 kg/cm^2 horizontal stress on average. Since no measured virgin stresses are available, the simulated stresses cannot be compared to the actual field stresses.

The analysis is terminated at day 140 since the closure rate is considered to be constant. The output for vertical closure and horizontal closure histories are shown in Figure 4.11 and Figure 4.12 respectively. The vertical stress history of wall and pillars is shown in Figure 4.13. The computed closures at the middle of the rooms are then compared with the field measurement, as indicated in Figure 4.14, Figure 4.15, Figure 4.16, and Figure 4.17 for vertical closures, horizontal closure of room 2105, horizontal closure of room 2104, and horizontal closure of room 2103 respectively. The comparison of vertical stress histories are shown in Figure 4.18, Figure 4.19, and Figure 4.20.

4.4.5 Discussion of results

Overall, the simulated closure of the rooms demonstrates a behaviour similar to the measured behaviour, for the following reasons:

- The simulated closing or possible failure of the rooms has the same sequence as the actual observation.
- Reloading effect while cutting the adjacent room is also produced by the simulated model.

The vertical stress history of pillars and wall are relatively close to the field readings. The discrepancies occurring at the early age of excavations might be caused by initial interaction between gauging equipment and the sorrounding rock.
However, the actual values of horizontal room closures are less than the actual observation. The differences arise due to the following aspects which are not provided by the model:

1. It is reported in reference [23] that numerous fractures along the maximum principal stress trajectory (about vertical) are observed in the laboratory model and in the actual yield pillar. These cracks are initiated by tensile stress. The crack length increases exponentially with increasing stress and the crack growth is time-dependent. Fractures a few meters in length and several centimeters in width were observed in the field. For these reasons, the field readings for horizontal room closures are higher than the analytical results.

2. As calculated in this study, the vertical stress in the pillars and wall increased from 230 kg/cm^2 to around 350 kg/cm^2. Since the ultimate strength of potash rock is of the range of 250 kg/cm^2 to 300 kg/cm^2, the pillar will be in the post peak or strain softening stage. In this stage, the strain is increasing exponentially.

3. The type of model used in this simulation is categorized as the *continuous model* [27]. In this model, the continuum is assumed to be free from any defect or, in other words, the rock is assumed to be *intact*. This assumption is, for the most part, far from the real condition. For example, the slip surface among the rock layers can increase horizontal movement of the pillars and walls. The other type of the models are the *discontinous model* and the *pseudo-continous model* [27], which represent a jointed rock continuum and a highly fractured/weathered rock continuum. The last two models take into account the discontinuities in their constitutive equations, which are beyond this study.

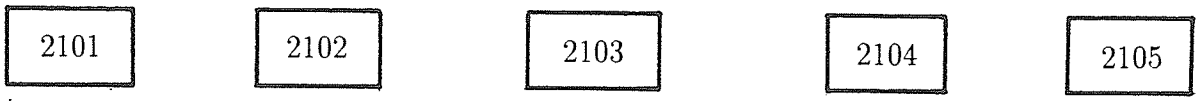

Feb. 17/84 May 12/84 June 4/84 Apr.30/84 Jan.23/84

Figure 4.8: Room configuration and completion dates

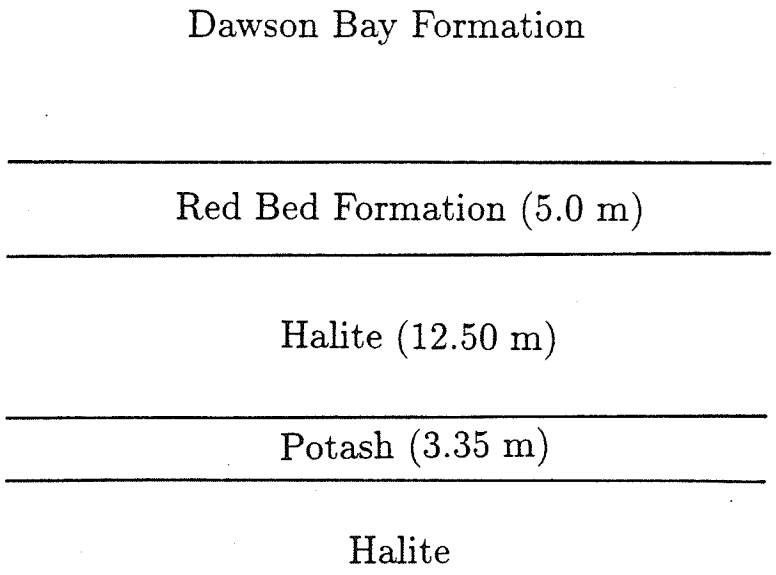

Figure 4.9: The assumed stratigraphy.

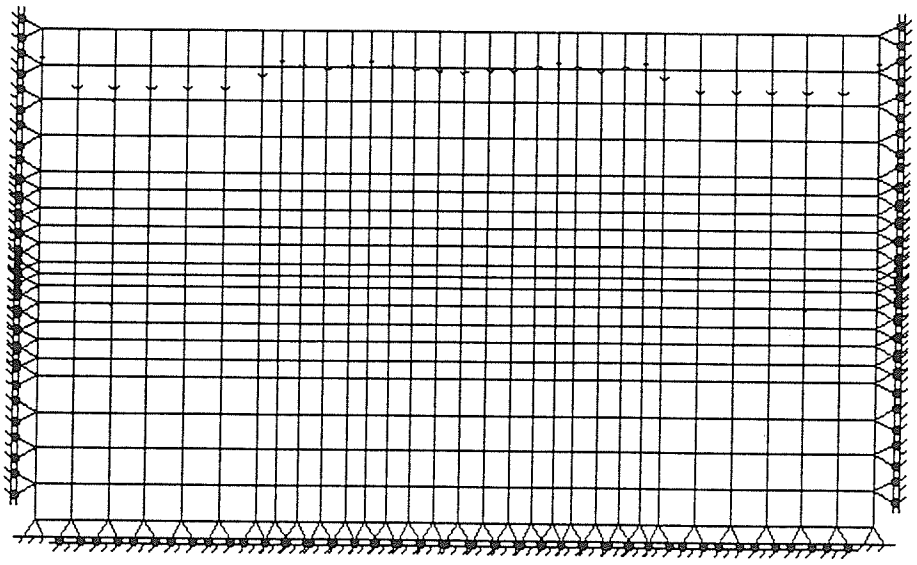

Figure 4.10: Finite element mesh of the mining.

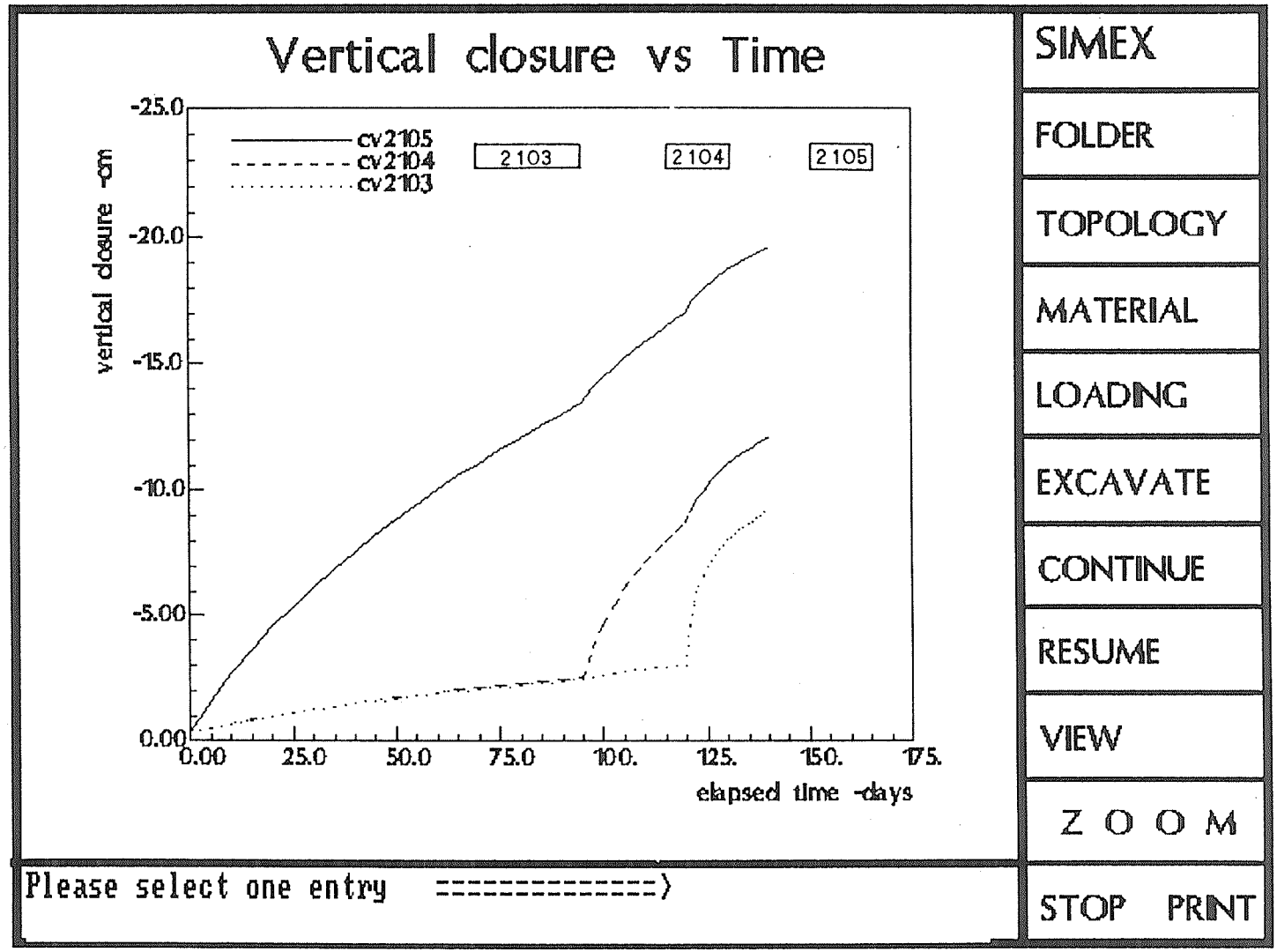

Figure 4.11: Computed vertical closures.

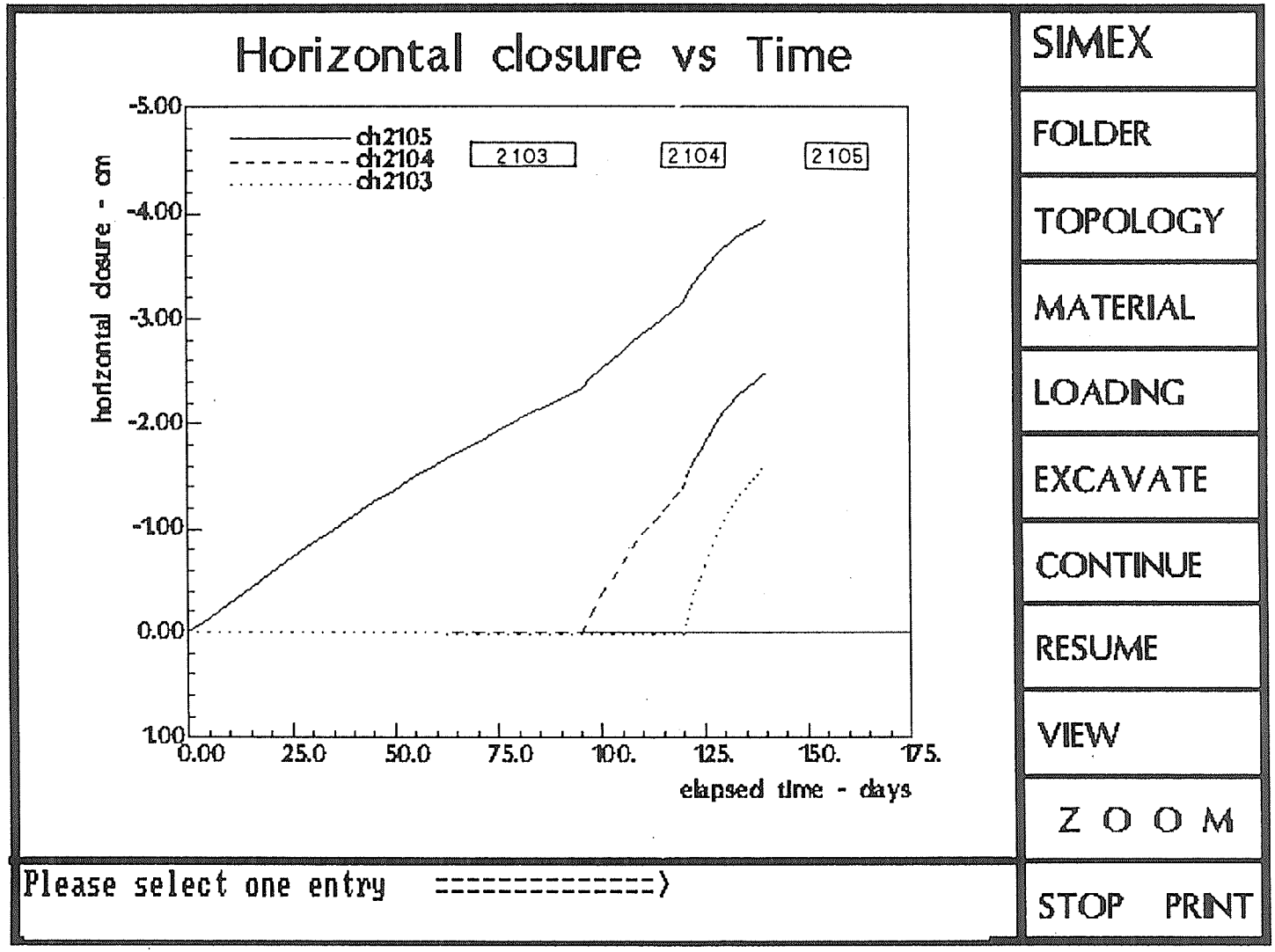

Figure 4.12: Computed horizontal closures.

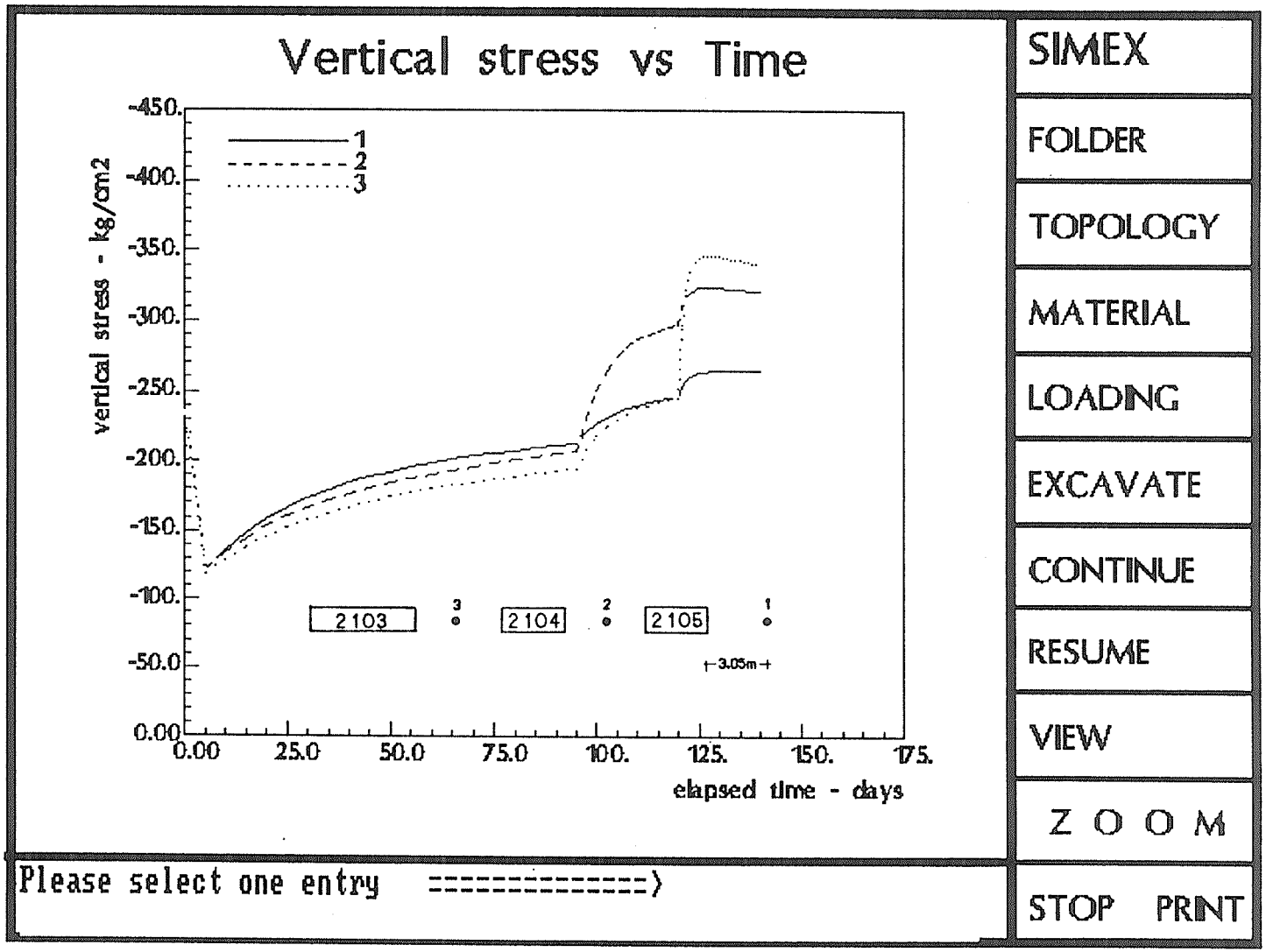

Figure 4.13: Computed vertical stress histories.

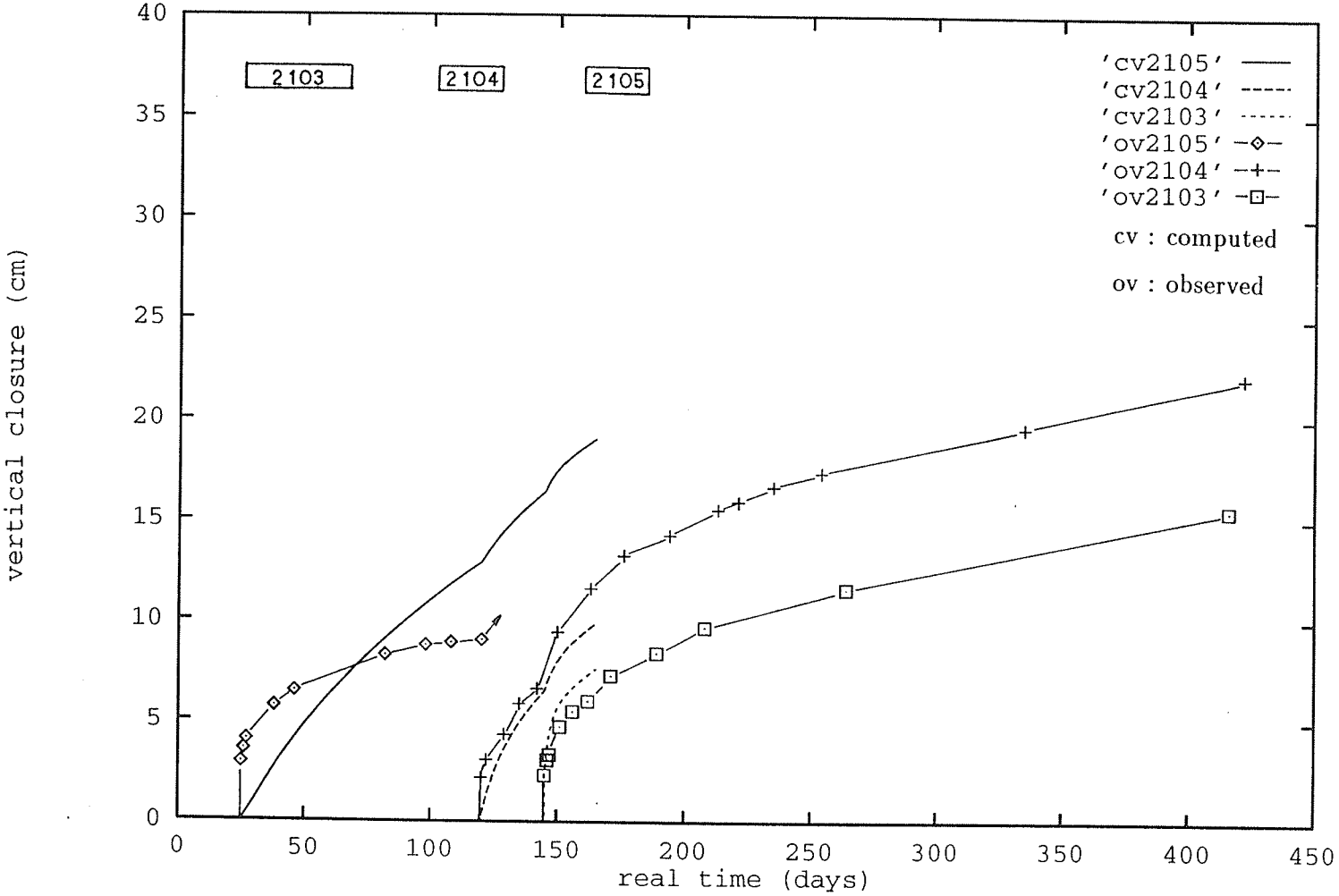

Figure 4.14: Computed and measured vertical closures.

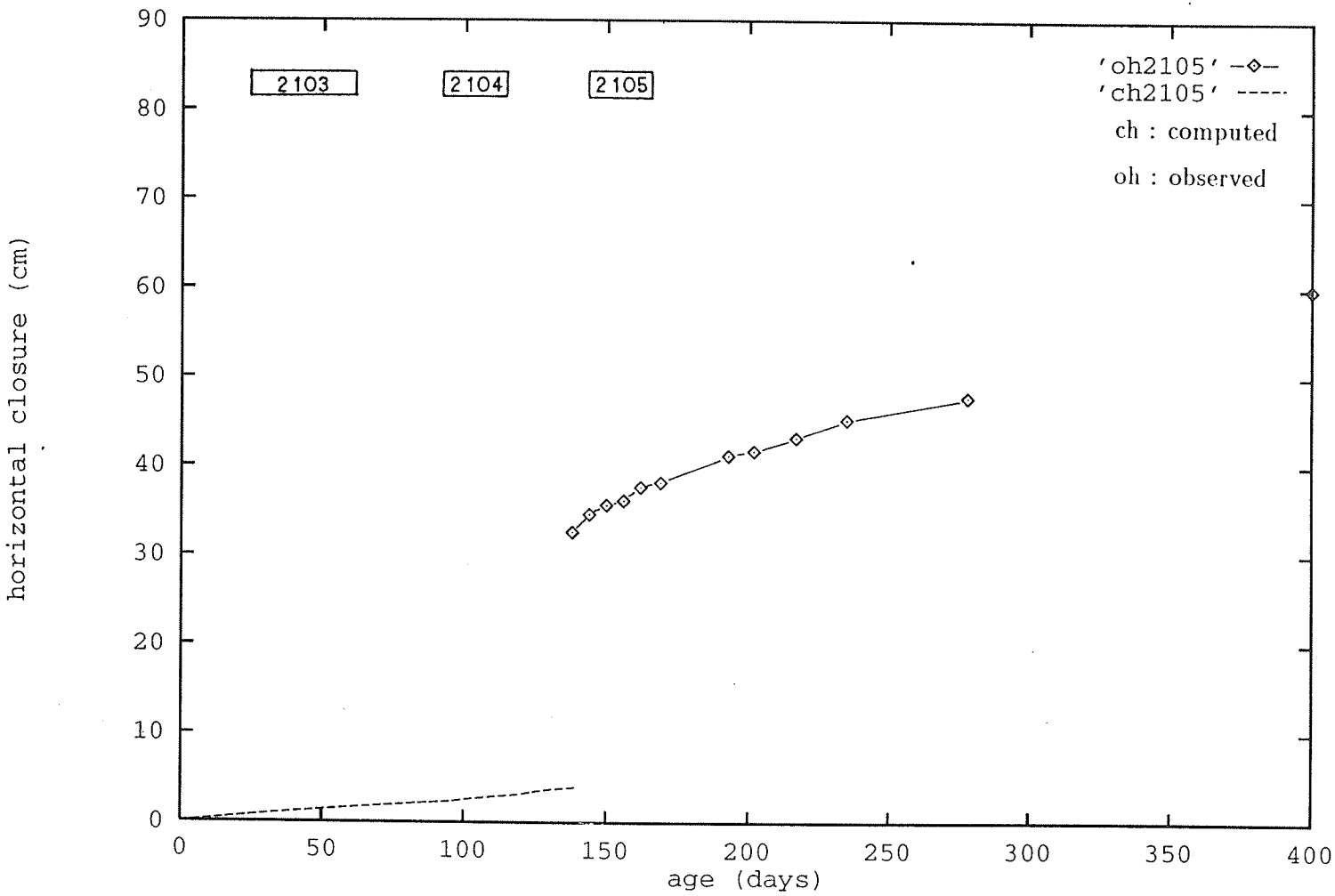

Figure 4.15: Computed and measured horizontal closures - 2105.

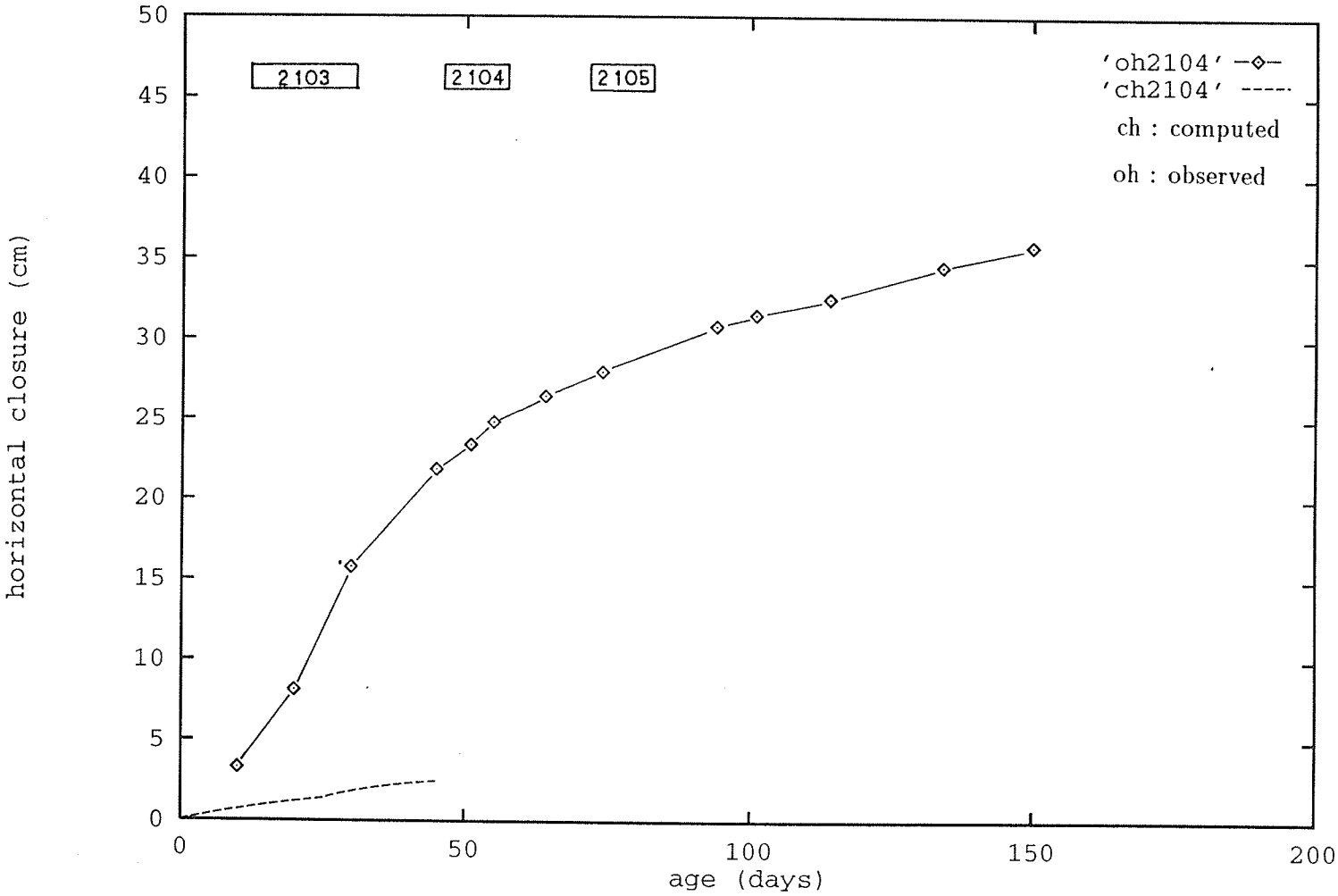

Figure 4.16: Computed and measured horizontal closures - 2104.

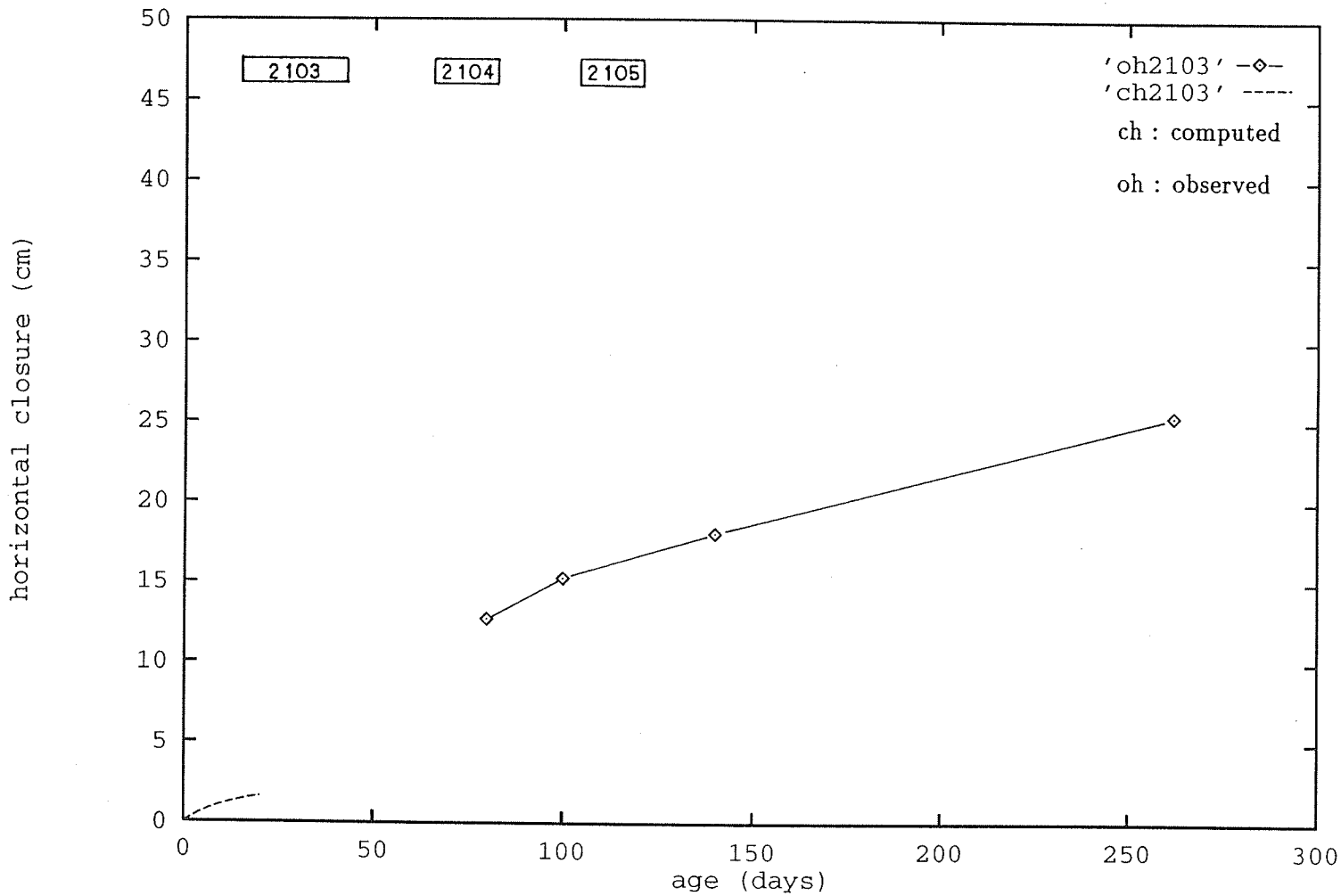

Figure 4.17: Computed and measured horizontal closures - 2103.

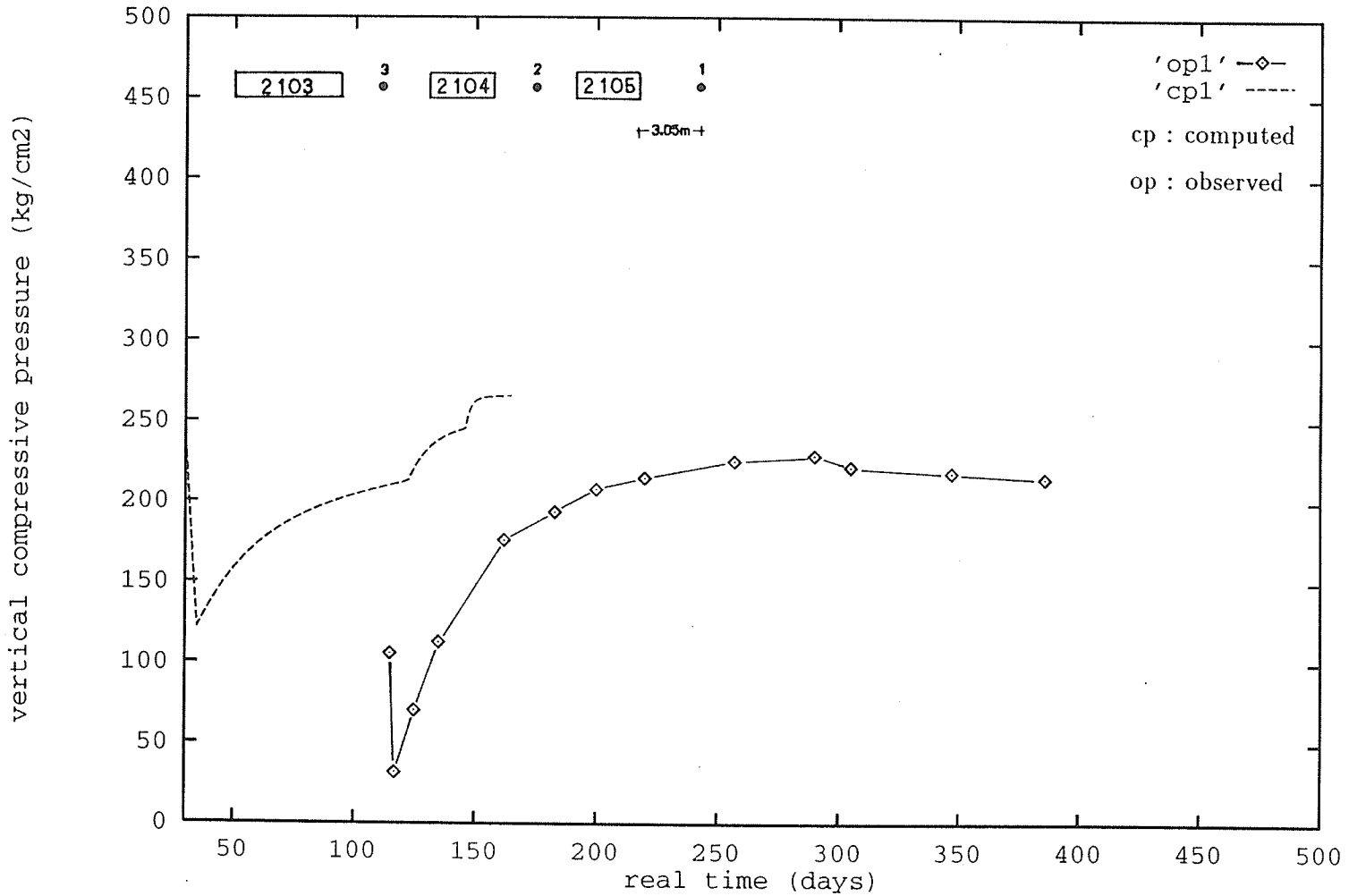

Figure 4.18: Vertical stress history - 2105 East wall.

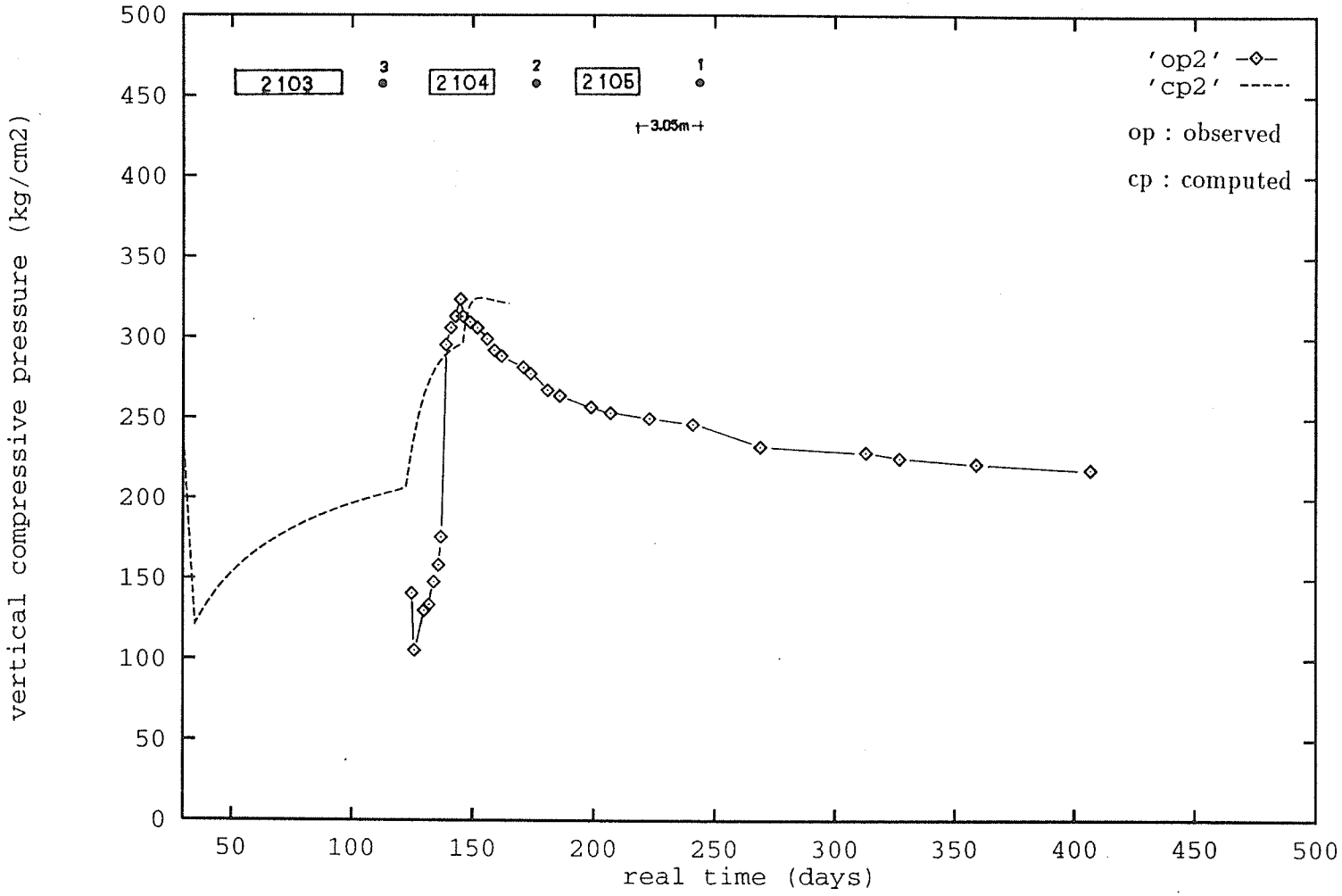

Figure 4.19: Vertical stress history - 2105/2104 Pillar.

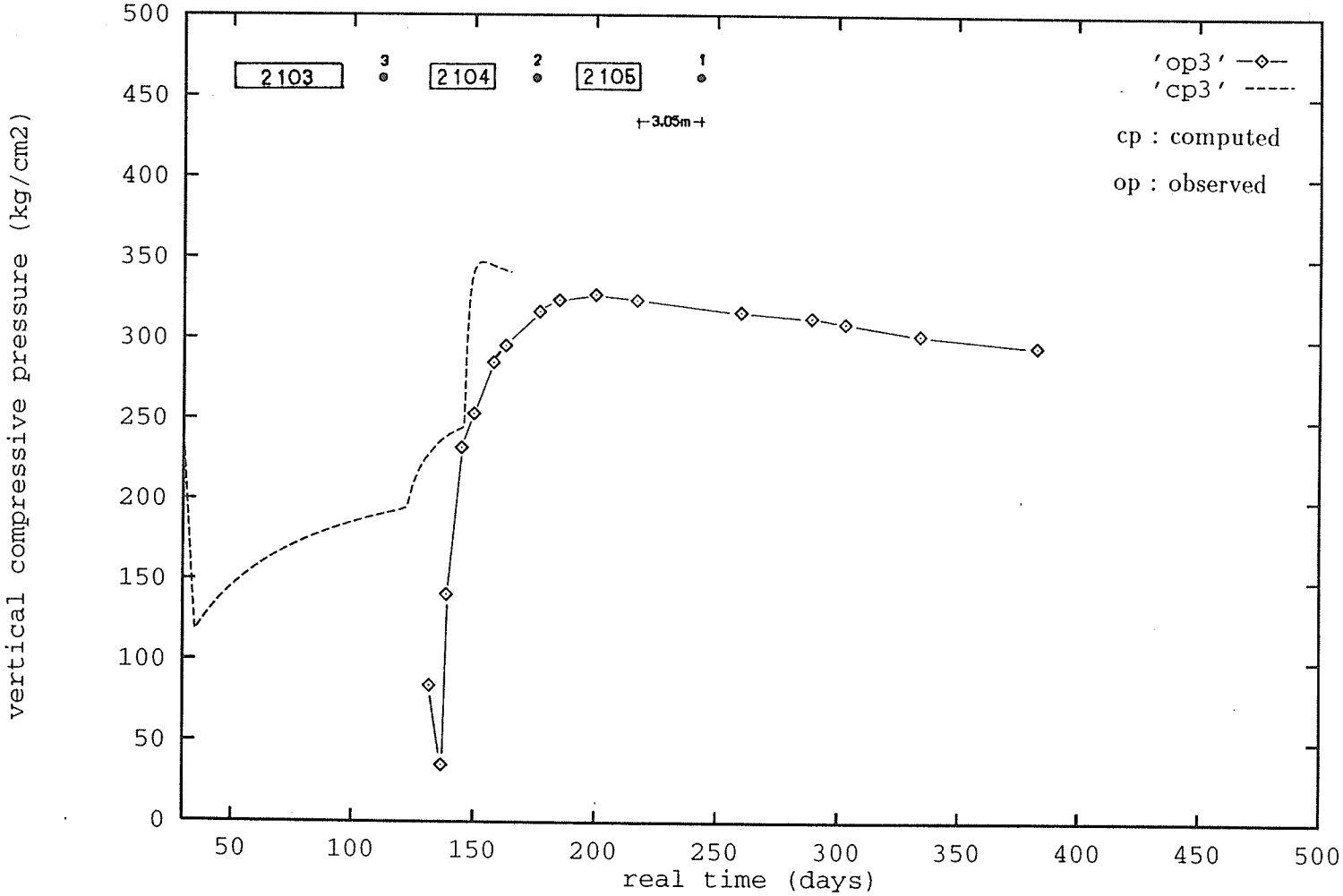

Figure 4.20: Vertical stress history - 2104/2103 Pillar.

Chapter 5

Conclusions and Future Research

5.1 Conclusions

The findings of chapter four confirmed that elasto-viscoplasticity theory is a most powerful tool to model the mining excavation processes. The main drawback of this approach consists of the difficulty of choosing the proper parameters which govern the time-dependent behaviour of potash in the mining field.
Through this engineering study, the following conclusions can be drawn;

1. Comparatively, the model gives a good approximation of vertical room closures and stresses in potash mining processes.

2. Elasto-viscoplasticity is a unified solution approach to a wide range of materally non-linear and time-dependent problems.

3. The overlay system gives more flexibility in approaching complex material behaviour.

The following section proposes several enhancements which will lead to a systematic approach in modelling the mining excavation process.

5.2 Future research

This thesis focused on the modelling of the time-dependent behaviour of potash. As previously mentioned, the experimental evidence provided to the author were

carried out over a period of six months in the laboratorium. These tests results need to be extended to a period of roughly two years, in order to achieve the steady state response and subsequently attain the ultimate tertiary creep regime. The required information must be extrapolated to the mining field via proper correlation procedures. This can be achieved by setting a testing program involving different specimen sizes where the size-effect issue can systematically investigated.
In order to properly trace the room-closure histories, several key components have to be modeled with a certain degree of reliability. These component are:

1. **Modelling of the clay seams**

   The clay seams must be accounted for using proper numerical tools. The use of small finite elements does not provide accurate stresses due to the "bad" aspect ratio of these elements. However, special interface elements equiped with a proper material law has to be incorporated in the model to capture the slip responsible of an important part of the overall global response.

2. **Modelling of the tertiary creep stage**

   Based on Figure 5.1, the viscoplastic model proposed in chapter three is capable of predicting the three creep stages. This fact can be illustrated by working out a simple trilinear model. Investigation of the stresses in the yield pillars shows that such modelling is necessary.

   Capabilities to account for linear strain hardening and softening have been successfully implemented in a version of the program. However, no validation is provided by experimental testing available. As such, it is recommended to pursue the efforts of Lajtai and co-worker [19] to bring the full response history to modelling.

3. **Fracture characterization**

   The underestimated horizontal closure is primarily due to the lack of accounting for cracking. The pillars undergo strain reversals due to cracking [18], [22],

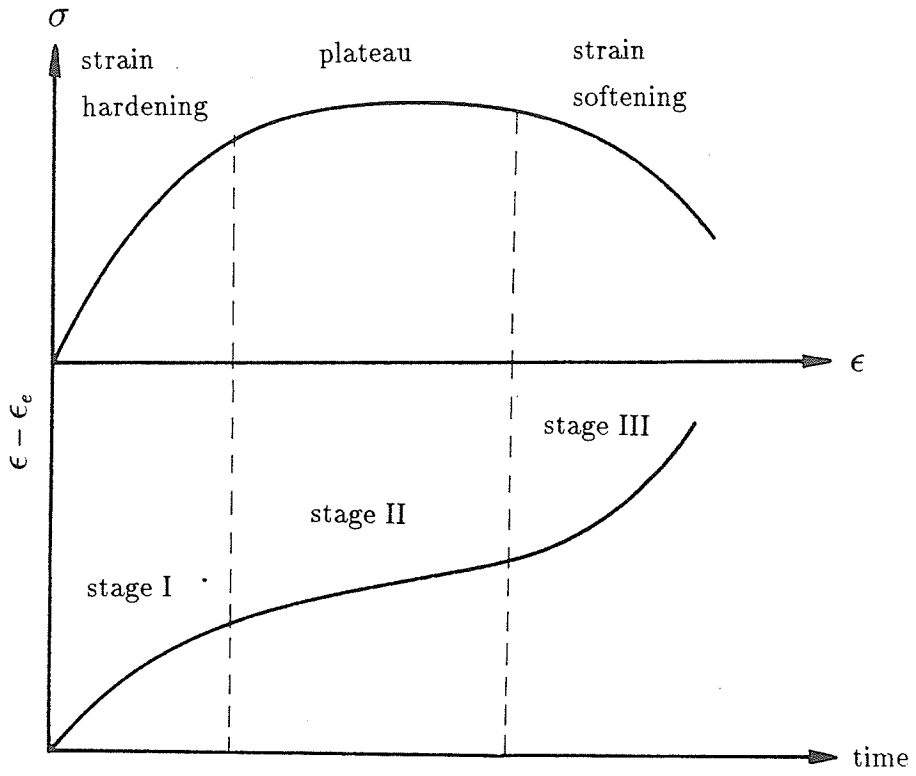

Figure 5.1: Stress-strain and creep curves.

[23]. This was not targeted in the current investigation. A realistic approach to correct for this would be to introduce discrete cracking. Time-dependent fracture characterization will be required for modelling purposes, such as ratio of crack extension, direction of crack propagation etc.

4. **Infinite elements, Initial stress, and Generalized plane strain condition**

   Infinite elements would be an elegant way of representing the true situation in the mine. This will require the use of "initial stress" type of load to maintain the required and direction of the confining pressure.

   The generalized plane strain condition where the out-of-plane stress level is maintained, would bring further information to the global behaviour of the mine structure.

Bibliography

[1] Ayari, M.L., *Simulation of Mining Excavation (SIMEX) Program*, Mechanical and Industrial Department, University of Manitoba, 1991.

[2] Chen, W.F. and Saleeb, A.F.,*Constitutive Equation for Engineering Materials*, V. 1, John Wiley, 1982.

[3] Malvern, L.E.,*Introduction to the Mechanics of a Continous Medium*, Prentice Hall, 1969.

[4] Johnson, W. and Mellor, P.B.,*Engineering Plasticity*, Van Nostrand Reinhold Company, 1973.

[5] Valliappan, S.,*Continuum Mechanics Fundamentals*, Balkema, 1981.

[6] Owen, D.R.J. and Hinton, E.,*Finite Elements in Plasticity*, Pineridge Press Limited, 1982.

[7] Olzak, W., Mroz, Z. and Perzyna, P.,*Recent Trends in the Development of the Theory of Plasticity*, Pergamon Press, 1963.

[8] Hill, R., *The Mathematical Theory of Plasticity*, first ed., Oxford University Press, 1956.

[9] Telles, J.C.F., *The Boundary Element Method Applied to Inelastic Problems*, Springer-Verlag, 1983.

[10] Cormeau, I.C., *Numerical stability in quasistatic elasto-viscoplasticity*, International Journal of Numerical Method in Engineering, 9,1975,pp 109-127.

[11] Stricklin, J.A., Hasler, W. and Teisemann, W., *Evaluation of solution procedures of material and/or geometrically non-linear structural analysis*, AIAA J. 11,1973,pp 292-299.

[12] Zienkiewicz, O.C., Cormeau, I.C., *Visco-plasticity - Plasticity and Creep in Elastic Solids - A Unified Numerical Solution Approach*, International Journal for Numerical Methods in Engineering, 8,1974,pp 821-845.

[13] Stolle, D.F.E., Higgins, J.E., *Viscoplasticity and Plasticity - Numerical Stability Revisited*, Proceeding of the International Symposium on Numerical Models in Geomechanics (NUMOG III), Elsevier, 1989, pp 431-438.

[14] Hughes, T.J.R., Taylor, R.L., *Unconditionally Stable Algorithm for Elasto/viscoplastic Finite Element Analysis*, Computers and Structures, 1978, 8,pp 169-173.

[15] Marques, J.M.M.C., Owen, D.R.J., *Implicit-Explicit Time Integration in Quasistatic Elastoviscoplasticty using Finite and Infinite Elements*, Computational Methods in Applied Mechanics, 1984, 42,pp 167-182.

[16] Owen, D.R.J., Prakash, A., Zienkiewicz, O.C., *Finite Element Analysis of Nonlinear Composite Materials by Use of Overlay Systems*, Computers and Structures, 4,1974,pp 1251-1267.

[17] Pande, G.N., Owen, D.R.J., Zienkiewicz, O.C., *Overlay Models in Time-Dependent Non-Linear Material Analysis*, Computers and Structures, 7,1977,pp 435-443.

[18] Lajtai, E.Z., *Fracture in Potash*, NSERC Research Partnership Program, The University of Manitoba and The Potash Corporation of Saskatchewan Cominco Fertilizer Ltd., 1991

[19] Duncan, E.J.S., Lajtai, E.Z., *The Creep of Saskatchewan Potash Rock in Uniaxial Compression*, Fracture in Potash, NSERC Research Partnership Program, The University of Manitoba and The Potash Corporation of Saskatchewan Cominco Fertilizer Ltd., 1991,pp 20-41.

[20] Duncan, E.J.S., *Deformation and Strength of Saskatchewan Potash Rock*, Ph.D. thesis, Department of Geological Engineering, University of Manitoba, 1990.

[21] Carter, B.J., *Physical and Numerical Modeling of Fracture in Rock: with special emphasis on the Potash Mines of Saskatchewan*, Ph.D. thesis, Department of Civil Engineering, University of Manitoba, 1992.

[22] Lajtai, E.Z., Carter, B.J., and Ayari, M.L., *Criteria for Brittle Fracture in Compression*, Engineering Fracture Mechanics, v.37,1992,pp 59-74.

[23] Lajtai, E.Z., Carter, B.J. *Time and Stress Dependence of Fracture Propagation in Potash Rock*, Fracture in Potash, NSERC Research Partnership Program, The University of Manitoba and The Potash Corporation of Saskatchewan Cominco Fertilizer Ltd., 1991, pp 42 - 52.

[24] Stimpson, B., Lajtai, E.Z., and Ayari, M.L., *Rock Mechanics of Potash Mining in Saskatchewan - In situ, Laboratory, and Computer Modelling Studies*, Proceeding of the CIM 94th. General meeting, Montreal, April 26 - 30, 1992.

[25] Ong, V., *Fax to Dr. Ayari. M.L.*, Potash Corporation of Saskatchewan Inc., Nov. 22,1991.

[26] Cominco Ltd., *Collection and Evaluation of Field Data Around Excavations in Potash to Evaluate Excavation Performance or Concept for New Mining Layouts*, Contract Serial Number OSQ83-00320, 1985.

[27] Sakurai, S., Ine, T., Shinji, M., *Finite Element Analysis of Discontinous Geological Materials in Association with Field Observation*, Numerical Method in Geomechanics, 1988, 3, pp 2029-2042.